

Vector meson spectral function and dilepton production rate in a hot and dense medium within an effective QCD approach

Chowdhury Aminul Islam, Sarbani Majumder, Najmul Haque and Munshi G. Mustafa

*Theory Division, Saha Institute of Nuclear Physics,
1/AF Bidhan Nagar, Kolkata-700064, India*

E-mail: chowdhury.aminulislam@saha.ac.in,
sarbani.majumder@saha.ac.in, najmul.haque@saha.ac.in,
munshigolam.mustafa@saha.ac.in

ABSTRACT: The properties of the vector meson current-current correlation function and its spectral representation are investigated in details with and without isoscalar-vector interaction within the framework of effective QCD approach, namely Nambu-Jona-Lasinio (NJL) model and its Polyakov Loop extended version (PNJL), at finite temperature and finite density. The influence of the isoscalar-vector interaction on the vector meson correlator is obtained using the ring resummation known as the Random Phase Approximation (RPA). The spectral as well as the correlation function in PNJL model show that the vector meson retains its bound property up to a moderate value of temperature above the phase transition. Using the vector meson spectral function we, for the first time, obtained the dilepton production rate from a hot and dense medium within the framework of PNJL model that takes into account the nonperturbative effect through the Polyakov Loop fields. The dilepton production rate in PNJL model is enhanced compared to NJL and Born rate in the deconfined phase due to the suppression of color degrees of freedom at moderate temperature. The presence of isoscalar-vector interaction further enhances the dilepton rate over the Born rate in the low mass region. Further, we also have computed the Euclidean correlation function in vector channel and the conserved density fluctuation associated with temporal correlation function appropriate for a hot and dense medium. The dilepton rate and the Euclidean correlator are also compared with available lattice data and those quantities in PNJL model are found to agree well in certain domain.

KEYWORDS: Quark-Gluon Plasma, Phenomenological Models, QCD

ARXIV EPRINT: [1411.6407](https://arxiv.org/abs/1411.6407)

Contents

1	Introduction	1
2	Some generalities	4
2.1	Correlation function and its spectral representation	4
2.2	Vector spectral function and dilepton rate	5
2.3	Temporal Euclidean correlation function and response to conserved density fluctuation	5
3	Effective QCD models	5
3.1	NJL model	5
3.2	PNJL model	6
4	Vector meson correlator in ring resummation	7
4.1	Ring resummation at zero temperature and chemical potential	8
4.2	Ring resummation at finite temperature and chemical potential	8
4.3	Conserved density fluctuation in ring approximation	10
4.4	Vector correlation function in one-loop	10
4.4.1	Temporal part	11
4.4.2	Spatial part	13
5	Results	14
5.1	Gap equations and mean fields	14
5.2	Vector spectral function and dilepton rate	16
5.2.1	Without vector interaction ($G_V = 0$)	17
5.2.2	With vector interaction ($G_V \neq 0$)	19
5.3	Vector correlation function	22
5.4	Quark number susceptibility and temporal correlation function	23
6	Conclusion	24

1 Introduction

Quantum Chromodynamics (QCD) being the fundamental theory of strong interaction exhibits a very rich phase structure at extreme conditions, *i.e.*, high temperature and/or high density. It is now well established that at these conditions a transition from normal hadronic matter to a state of strongly interacting exotic quark gluon plasma (QGP) is possible [1, 2]. In recent years, a tremendous effort has been devoted to the creation of QGP in the laboratory. The heavy-ion collider experiments presently dedicated to this search are the Relativistic Heavy Ion Collider (RHIC) at Brookhaven National Laboratory (BNL) [3–6] and the Large Hadron Collider (LHC) at the European Organization for Nuclear Research (CERN) [7, 8]. Also, future fixed target experiments are planned

at the Facility for Antiproton and Ion Research (FAIR) at the Gesellschaft für Schwerionenforschung (GSI) [9]. In all these experiments heavy ions are accelerated to relativistic speeds in order to achieve such extreme conditions required for the creation of a short-lived QGP. Various diagnostic measurements at RHIC BNL [10–18] in the recent past have indicated a strong hint for the creation of a semi-QGP (not weakly interacting like usual QGP) within a first few fm/c of the collisions through the manifestation of hadronic final states. Also, new data from LHC CERN [19–23] have further consolidated the formation of such a state of matter.

One of the most interesting as well as promising subjects in the area of theoretical high energy physics is the study of the strongly interacting many particle system under these extreme conditions. Dynamical properties of many particle system are associated with the correlation function [24–26]. We know that many of the hadron properties are embedded in the correlation function and its spectral representation. Such properties in vacuum [27] are very well studied in QCD. The presence of a stable mesonic state is understood by the delta function like peak in the spectral function. At low temperature most of the hadronic models [28, 29] work well but break down near the phase transition temperature, T_c . While propagating through the hot and dense medium [30, 31], the vacuum properties of any particle get modified due to the change of its dispersion properties in the medium. The temporal correlation function is related to the response of the conserved density fluctuations due to the symmetry of the system. On the other hand, the spatial correlation function exhibits information on the masses and width. So, in a hot and dense medium the properties of hadrons, *viz.*, response to the fluctuations, masses, width, compressibility etc., will be affected. Hence, hadron properties at finite temperature and density are also encoded in the structure of its correlation function and the corresponding spectral representation, which may reflect the degrees of freedom around the phase transition point and thus the properties of the deconfined, strongly interacting matter. As for example, the spectral representation of the vector current-current correlation can be indirectly accessible by high energy heavy-ion experiments as it is related to the differential thermal cross section for the production of lepton pairs [30, 31]. Moreover, in the limit of small frequencies, various transport coefficients of the hot and dense medium can be determined from the spatial spectral representation of the vector channel correlation [30, 31]. The static limit of the temporal correlation function provides the response to the fluctuation of the conserved quantities. For a quasiparticle in the medium, the δ -like peak is expected to be smeared due to the thermal width, which increases with the increase in temperature. At sufficiently high temperature and density, the contribution from the mesonic state in the spectral function will be broad enough so that it is not very meaningful to speak of it as a well defined state any more [32–34].

At high temperature but zero chemical potential, the structure of the vector meson correlation function, determination of thermal dilepton rate and various transport coefficients have been studied using Lattice QCD (LQCD) framework at zero momentum [35–43] and also at nonzero momentum [44], which is a first principle calculation that takes into account the nonperturbative effects of QCD. Such studies for hot and dense medium are also performed within perturbative techniques like Hard Thermal Loop (HTL) approxima-

tion [45–58], and in dimensional reduction [59, 60] appropriate for weakly interacting QGP. Nevertheless, at RHIC and LHC energies the maximum temperature reached is not very far from the phase transition temperature T_c and a hot and dense matter created in these collisions is nonperturbative in nature (semi-QGP). So, most of the perturbative methods may not be applicable in this temperature domain but these methods, however, are very reliable and accurate at very high temperature [61–64] for usual weakly interacting QGP. In effective QCD model framework [32, 33, 65–69], several studies have also been done in this direction. Mesonic spectral functions and the Euclidean correlator in scalar, pseudoscalar and vector channel have been discussed in refs. [65–69] using Nambu-Jona-Lasinio (NJL) model. The NJL model has no information related to the confinement and thus does not have any nonperturbative effect associated with the semi-QGP above T_c . However, the Polyakov Loop extended NJL (PNJL) model [70, 71] contains nonperturbative information through Polyakov Loop [72–79] that suppresses the color degrees of freedom as the Polyakov Loop expectation value decreases when $T \rightarrow T_c^+$. The thermodynamic properties of strongly interacting matter have been studied extensively within the framework of NJL and PNJL models [80–84]. The properties of the mesonic correlation functions have also been studied in scalar and pseudoscalar channel using PNJL model in refs. [85, 86]. We intend to study, for the first time in PNJL model, the properties of the vector correlation function and its spectral representation to understand the nonperturbative effect on the spectral properties, e.g., the dilepton production rate and the conserved density fluctuations, in a hot and dense matter created in heavy-ion collisions.

Further, the low temperature and high density part of the phase diagram is still less explored compared to the high temperature one. At finite densities the effect of chirally symmetric vector channel interaction becomes important and it is established that within the NJL or PNJL model this type of interaction weakens the first order transition line [87–92] in contrary to the scalar coupling which tends to favor the appearance of first order phase transitions. It is important to mention here that the determination of the strength of vector coupling constant is crucial under model formalism. It cannot be fixed using vector meson mass as it is beyond the characteristic energy cut-off of the model. However, at the same time incorporation of vector interaction is important if one intends to study the various spectral properties of the system at non-zero chemical potential [68, 93] appropriate for FAIR scenario [9]. In the present work, we study the nonperturbative effect of Polyakov Loop, along with the presence as well as the absence of the repulsive isoscalar-vector interaction, on the spectral function, correlation function and various spectral properties, (e.g., the rate of dilepton production, fluctuation of conserved charges) in a hot and dense matter. The influence of this repulsive vector channel interaction on the correlator and its spectral representation has been obtained using ring resummation. The results are compared with NJL model and the available lattice QCD (LQCD) data.

The paper is organized as follows: in section 2 we will briefly outline some of the generalities related to the correlation function and its spectral representation, and their relations to various physical quantities we would like to study. In section 3 we briefly sketch the effective models namely NJL and PNJL model. In section 4 we obtain the vector correlation function and its spectral properties through the isoscalar-vector interaction

within the ring resummation both in vacuum as well as in a hot and dense medium. We present our findings relevant for a hot and dense medium in section 5 and finally, conclude in section 6.

2 Some generalities

2.1 Correlation function and its spectral representation

In general the correlation function in coordinate space is given by

$$\mathcal{G}_{AB}(t, \vec{x}) \equiv \mathcal{T}(\hat{A}(t, \vec{x})\hat{B}(0, \vec{0})) = \int \frac{d\omega}{2\pi} \int \frac{d^3q}{(2\pi)^3} e^{i\omega t - i\vec{q}\cdot\vec{x}} \mathcal{G}_{AB}(\omega, \vec{q}), \quad (2.1)$$

where \mathcal{T} is the time-ordered product of the two operators \hat{A} and \hat{B} , and the four momentum $Q \equiv (\omega, \vec{q})$ with $q = |\vec{q}|$.

By taking the Fourier transformation one can obtain the momentum space correlation function as

$$\mathcal{G}_{AB}(\omega, \vec{q}) = \int dt \int d^3\vec{x} \mathcal{G}_{AB}(t, \vec{x}) e^{-i\omega t + i\vec{q}\cdot\vec{x}}. \quad (2.2)$$

The thermal meson current-current correlator in Euclidean time $\tau \in [0, \beta = 1/T]$ is given as [45, 94]

$$\mathcal{G}_M^E(\tau, \vec{x}) = \langle \mathcal{T}(J_M(\tau, \vec{x})J_M^\dagger(0, \vec{0})) \rangle_\beta = T \sum_{n=-\infty}^{\infty} \int \frac{d^3q}{(2\pi)^3} e^{-i(\omega_n \tau + \vec{q}\cdot\vec{x})} \mathcal{G}_M^E(i\omega_n, \vec{q}), \quad (2.3)$$

where the mesonic current is defined as $J_M = \bar{\psi}(\tau, \vec{x})\Gamma_M\psi(\tau, \vec{x})$, with $\Gamma_M = 1, \gamma_5, \gamma_\mu, \gamma_\mu\gamma_5$ for scalar, pseudoscalar, vector and pseudovector channel respectively. The momentum space correlator $\mathcal{G}_M^E(i\omega_n, \vec{q})$ at the discrete Matsubara modes $\omega_n = 2\pi nT$ can be obtained as

$$\mathcal{G}_M^E(i\omega_n, \vec{q}) = - \int_{-\infty}^{\infty} d\omega \frac{\sigma_M(\omega, \vec{q})}{i\omega_n - \omega}. \quad (2.4)$$

The spectral function $\sigma_H(\omega, \vec{q})$ for a given mesonic channel H , can be obtained from the imaginary part of the momentum space Euclidean correlator in (2.4) by analytic continuation as

$$\sigma_H(\omega, \vec{q}) = \frac{1}{\pi} \text{Im} \mathcal{G}_H^E(i\omega_n = \omega + i\epsilon, \vec{q}), \quad (2.5)$$

where $H = 00, ii$ and V stand for temporal, spatial and vector spectral function, respectively. The vector spectral function is expressed in terms of temporal and spatial components as $\sigma_V = \sigma_{00} - \sigma_{ii}$.

Using (2.3) and (2.4) one obtains the spectral representation of the thermal correlation function in Euclidean time but at a fixed momentum \vec{q} as

$$\mathcal{G}_H^E(\tau, \vec{q}) = \int_0^\infty d\omega \sigma_H(\omega, \vec{q}) \frac{\cosh[\omega(\tau - \beta/2)]}{\sinh[\omega\beta/2]}. \quad (2.6)$$

Because of the difficulty in analytic continuation in LQCD the spectral function can not be obtained directly using (2.5). Instead a calculation in LQCD proceeds by evaluating the Euclidean correlation function. Using a probabilistic application based on maximum entropy method (MEM) [95–97], (2.6) is then inverted to extract the spectral function and thus various spectral properties are computed in LQCD.

2.2 Vector spectral function and dilepton rate

The vector meson spectral function, σ_V , and the differential dilepton production rate are related as [45]

$$\frac{dR}{d^4x d^4Q} = \frac{5\alpha^2}{54\pi^2} \frac{1}{M^2} \frac{1}{e^{\omega/T} - 1} \sigma_V(\omega, \vec{q}), \quad (2.7)$$

where the invariant mass of the lepton pair is $M^2 = \omega^2 - q^2$ and α is the fine structure constant.

2.3 Temporal Euclidean correlation function and response to conserved density fluctuation

The quark number susceptibility (QNS), χ_q measures of the response of the quark number density ρ with infinitesimal change in the quark chemical potential, $\mu + \delta\mu$ and is related to temporal correlation function through fluctuation dissipation theorem [68] as

$$\begin{aligned} \chi_q(T) &= \left. \frac{\partial \rho}{\partial \mu} \right|_{\mu=0} = \int d^4x \langle J_0(0, \vec{x}) J_0(0, \vec{0}) \rangle \\ &= \lim_{\vec{q} \rightarrow 0} \beta \int \frac{d\omega}{2\pi} \frac{-2}{1 - e^{-\omega/T}} \text{Im} \mathcal{G}_{00}(\omega, \vec{q}) = -\lim_{\vec{q} \rightarrow 0} \text{Re} \mathcal{G}_{00}(\omega = 0, \vec{q}), \end{aligned} \quad (2.8)$$

where Kramers-Kronig dispersion relation has also been used.

The quark number conservation implies that $\lim_{\vec{q} \rightarrow 0} \text{Im} \mathcal{G}_{00}(\omega, \vec{q}) \propto \delta(\omega)$ and the temporal spectral function in (2.5) becomes

$$\sigma_{00}(\omega, \vec{0}) = \frac{1}{\pi} \text{Im} \mathcal{G}_{00}(\omega, \vec{0}) = -\omega \delta(\omega) \chi_q(T). \quad (2.9)$$

The relation of the Euclidean temporal correlation function and the response to the fluctuation of conserved number density, χ_q , can be obtained from (2.6) as

$$\mathcal{G}_{00}^E(\tau T) = -T \chi_q(T), \quad (2.10)$$

which is independent of the Euclidean time, τ , but depends on T .

3 Effective QCD models

3.1 NJL model

In the present work we consider 2 flavor NJL model with vector channel interaction. The corresponding Lagrangian is [27, 68, 98–100]:

$$\mathcal{L}_{\text{NJL}} = \bar{\psi}(i\gamma_\mu \partial^\mu - m_0)\psi + \frac{G_S}{2} [(\bar{\psi}\psi)^2 + (\bar{\psi}i\gamma_5\vec{\tau}\psi)^2] - \frac{G_V}{2} (\bar{\psi}\gamma_\mu\psi)^2, \quad (3.1)$$

where, $m_0 = \text{diag}(m_u, m_d)$ with $m_u = m_d$ and $\vec{\tau}$'s are Pauli matrices. G_S and G_V are the coupling constants of local scalar type four-quark interaction and isoscalar-vector interaction respectively.

The scalar four quark interaction term leads to the formation of chiral condensate $\sigma = \langle \bar{\psi}\psi \rangle$. The condensate resulting from the additional vector coupling term only contains the time like component and the corresponding condensate is $n = \langle \bar{\psi}\gamma^0\psi \rangle$ [88, 100]. The thermodynamic potential in mean field approximation is given as:

$$\Omega_{\text{NJL}} = \frac{G_S}{2}\sigma^2 - \frac{G_V}{2}n^2 - 2N_f N_c \int_{\Lambda} \frac{d^3p}{(2\pi)^3} E_p - 2N_f N_c T \int \frac{d^3p}{(2\pi)^3} \left[\ln(1 + e^{-(E_p - \tilde{\mu})/T}) + \ln(1 + e^{-(E_p + \tilde{\mu})/T}) \right]. \quad (3.2)$$

Here $E_p = \sqrt{\vec{p}^2 + M_f^2}$ is the energy of a quark with flavor f having constituent mass or the dynamical mass M_f and Λ is a finite three momentum cut-off. The thermodynamic potential depends on the dynamical fermion mass M_f and the modified quark chemical potential $\tilde{\mu}$ which are related to the scalar (σ) and vector (n) condensates through the relations

$$M_f = m_0 - G_S \sigma, \quad (3.3)$$

and

$$\tilde{\mu} = \mu - G_V n, \quad (3.4)$$

respectively.

3.2 PNJL model

Let us now briefly discuss PNJL model [80–84, 90], where, unlike NJL model we have a couple of more mean fields in the form of the expectation value of the Polyakov Loop fields¹ Φ and its conjugate $\bar{\Phi}$. The Lagrangian for the 2 flavor PNJL model with vector channel interaction is given by,

$$\mathcal{L}_{\text{PNJL}} = \bar{\psi}(i\not{D} - m_0 + \gamma_0\mu)\psi + \frac{G_S}{2}[(\bar{\psi}\psi)^2 + (\bar{\psi}i\gamma_5\vec{\tau}\psi)^2] - \frac{G_V}{2}(\bar{\psi}\gamma_\mu\psi)^2 - \mathcal{U}(\Phi[A], \bar{\Phi}[A], T), \quad (3.5)$$

¹We recall that the Polyakov Loop expectation value Φ acts as an order parameter [72–79] for pure $SU(N_c)$ gauge theory. Given the role of an order parameter, if $\Phi(\bar{\Phi}) = 0$ the center symmetry $Z(N_c)$ of $SU(N_c)$ is unbroken and there is no ionization of $Z(N_c)$ charge, which is the confined phase below a certain temperature. At high temperature the $Z(N_c)$ symmetry is spontaneously broken, $\Phi(\bar{\Phi}) \neq 0$ corresponds to a deconfined phase of gluonic plasma and there are N_c different equilibrium states distinguished by the phase $2\pi j/N_c$ with $j = 0, \dots, (N_c - 1)$. We also note that the $Z(N_c)$ symmetry is explicitly broken in presence of dynamical quark, yet it can be considered as an approximate symmetry and Φ can still provide useful information as an order parameter [101].

a_0	a_1	a_2	a_3	b_3	b_4	κ
6.75	-1.95	2.625	-7.44	0.75	7.5	0.1

Table 1. Parameter set used in this work for the Polyakov Loop potential and the Vander Monde term.

where $D^\mu = \partial^\mu - ig\mathcal{A}_a^\mu\lambda_a/2$, \mathcal{A}_a^μ being the SU(3) background fields and λ_a 's are the Gell-Mann matrices. The thermodynamic potential can be obtained as [80–83]

$$\begin{aligned}
 \Omega_{\text{PNJL}} = & \mathcal{U}(\Phi, \bar{\Phi}, T) + \frac{G_S}{2}\sigma^2 - \frac{G_V}{2}n^2 \\
 & - 2N_f T \int \frac{d^3p}{(2\pi)^3} \ln \left[1 + 3 \left(\Phi + \bar{\Phi} e^{-(E_p - \bar{\mu})/T} \right) e^{-(E_p - \bar{\mu})/T} + e^{-3(E_p - \bar{\mu})/T} \right] \\
 & - 2N_f T \int \frac{d^3p}{(2\pi)^3} \ln \left[1 + 3 \left(\bar{\Phi} + \Phi e^{-(E_p + \bar{\mu})/T} \right) e^{-(E_p + \bar{\mu})/T} + e^{-3(E_p + \bar{\mu})/T} \right] \\
 & - \kappa T^4 \ln[J(\Phi, \bar{\Phi})] - 2N_f N_c \int_\Lambda \frac{d^3p}{(2\pi)^3} E_p .
 \end{aligned} \tag{3.6}$$

The effective Polyakov Loop gauge potential is parametrized as

$$\frac{\mathcal{U}(\Phi, \bar{\Phi}, T)}{T^4} = -\frac{b_2(T)}{2}\Phi\bar{\Phi} - \frac{b_3}{6}(\Phi^3 + \bar{\Phi}^3) + \frac{b_4}{4}(\bar{\Phi}\Phi)^2, \tag{3.7}$$

with

$$b_2(T) = a_0 + a_1 \left(\frac{T_0}{T} \right) + a_2 \left(\frac{T_0}{T} \right)^2 + a_3 \left(\frac{T_0}{T} \right)^3 .$$

Values of different coefficients $a_0, a_1, a_2, a_3, b_3, b_4$ and κ have been tabulated [82, 85] in table 1. The Vandermonde determinant $J(\Phi, \bar{\Phi})$ is given as [82, 101]

$$J[\Phi, \bar{\Phi}] = \frac{27}{24\pi^2} \left[1 - 6\Phi\bar{\Phi} + 4(\Phi^3 + \bar{\Phi}^3) - 3(\Phi\bar{\Phi})^2 \right]. \tag{3.8}$$

We also note that the mass gap in (3.3) and the modified chemical potential in (3.4) will now have dependence on Φ and $\bar{\Phi}$ through σ and n .

4 Vector meson correlator in ring resummation

We intend here to consider the isoscalar-vector interaction. Generally, from the structure of the interaction one can write the full vector channel correlation function by a geometric progression of one-loop irreducible amplitudes [27]. In the present form of our model Lagrangian with effective coupling G_V , the Dyson-Schwinger equation (DSE) for the vector correlator $C_{\mu\nu}$ within the ring approximation as shown in figure 1 reads as

$$C_{\mu\nu} = \Pi_{\mu\nu} + G_V \Pi_{\mu\sigma} C_\nu^\sigma, \tag{4.1}$$

where $\Pi_{\mu\nu}$ is one loop vector correlator.

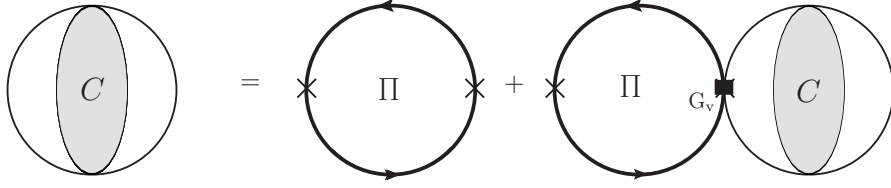


Figure 1. Vector correlator in ring resummation.

4.1 Ring resummation at zero temperature and chemical potential

The general properties of a vector correlation function at vacuum:

$$\Pi_{\mu\nu}(Q^2) = \left(g_{\mu\nu} - \frac{Q_\mu Q_\nu}{Q^2} \right) \Pi(Q^2), \quad (4.2)$$

$$C_{\mu\nu}(Q^2) = \left(g_{\mu\nu} - \frac{Q_\mu Q_\nu}{Q^2} \right) C(Q^2), \quad (4.3)$$

where $\Pi(Q^2)$ and $C(Q^2)$ are scalar quantities with $Q \equiv (q_0, \vec{q})$, is the four momentum.

Using (4.2) and (4.3), (4.1) can be reduced to a scalar DSE as

$$\begin{aligned} C &= \Pi + G_V \Pi C \\ C &= \frac{\Pi}{1 - G_V \Pi} \end{aligned} \quad (4.4)$$

The general structure of a vector correlator in vacuum becomes

$$C_{\mu\nu} = \frac{\Pi}{1 - G_V \Pi} \left(g_{\mu\nu} - \frac{Q_\mu Q_\nu}{Q^2} \right). \quad (4.5)$$

Using (4.5) the spectral representation in vacuum can be obtained from (2.5). The vacuum properties of vector meson can be studied using this spectral function [27] but we are interested in those at finite temperature and density appropriate for hot and dense medium formed in heavy-ion collisions and the vacuum, as we will see later, is in-built therein. Below we briefly outline how the vector correlation function and its spectral properties will be modified in a hot and dense medium.

4.2 Ring resummation at finite temperature and chemical potential

The general structure of one-loop and resummed vector correlation function in the medium (T and $\mu \neq 0$) can be decomposed [30, 31, 102] as:

$$\Pi_{\mu\nu}(Q^2) = \Pi_T(Q^2) P_{\mu\nu}^T + \Pi_L(Q^2) P_{\mu\nu}^L, \quad (4.6)$$

$$C_{\mu\nu}(Q^2) = C_T(Q^2) P_{\mu\nu}^T + C_L(Q^2) P_{\mu\nu}^L, \quad (4.7)$$

where $\Pi_{L(T)}$ and $C_{L(T)}$ are the respective scalar parts of $\Pi_{\mu\nu}$ and $C_{\mu\nu}$. $P_{\mu\nu}^{L(T)}$ are longitudinal (transverse) projection operators with their well defined properties in the medium and can be chosen as [102],

$$P_{\mu\nu}^L = \frac{Q^2}{\tilde{Q}^2} \bar{U}_\mu \bar{U}_\nu, \quad P_{\mu\nu}^T = \eta_{\mu\nu} - U_\mu U_\nu - \frac{\tilde{Q}_\mu \tilde{Q}_\nu}{\tilde{Q}^2}. \quad (4.8)$$

Here U_μ is the proper four velocity which in the rest frame of the heat bath has the form $U_\mu = (1, 0, 0, 0)$. $\tilde{Q}_\mu = (Q_\mu - \omega U_\mu)$ is the four momentum orthogonal to U_μ whereas $\bar{U}_\mu = (U_\mu - \omega Q_\mu/Q^2)$ is orthogonal component of U_μ 's with respect to the four momentum Q_μ . Also, the respective scalar parts, $\Pi_{L(T)}$, of $\Pi_{\mu\nu}$ are obtained as

$$\Pi_L = -\frac{Q^2}{q^2}\Pi_{00}; \quad \Pi_T = \frac{1}{(D-2)} \left[\frac{\omega^2}{q^2}\Pi_{00} - \Pi_{ii} \right], \quad (4.9)$$

where D , is the space-time dimension of the theory.

Using (4.6) and (4.7) in (4.1) one obtains

$$C_T(Q^2)P_{\mu\nu}^T + C_L(Q^2)P_{\mu\nu}^L = [\Pi_T + G_V\Pi_T C_T] P_{\mu\nu}^T + [\Pi_L + G_V\Pi_L C_L] P_{\mu\nu}^L. \quad (4.10)$$

Now, the comparison of coefficients on both sides leads to two scalar DSEs: One, for transverse mode, reads as

$$C_T = \frac{\Pi_T}{1 - G_V\Pi_T}, \quad (4.11)$$

and the other one, for the longitudinal mode, reads as:

$$C_L = \frac{\Pi_L}{1 - G_V\Pi_L} \quad (4.12)$$

Let us first write the temporal component of the resummed correlator: it is clear from (4.8) that $P_{00}^T = 0$. So we have from (4.7)

$$C_{00} = \frac{\Pi_L}{1 - G_V\Pi_L} P_{00}^L = \frac{\Pi_{00}}{1 + G_V\frac{Q^2}{q^2}\Pi_{00}}, \quad (4.13)$$

and the imaginary part of the temporal component of C_{00} is obtained as

$$\text{Im}C_{00} = \frac{\text{Im}\Pi_{00}}{\left[1 - G_V\left(1 - \frac{\omega^2}{q^2}\right)\text{Re}\Pi_{00}\right]^2 + \left[G_V\left(1 - \frac{\omega^2}{q^2}\right)\text{Im}\Pi_{00}\right]^2}. \quad (4.14)$$

The spatial component of the resummed correlator (C_{ii}) can be written as:

$$C_{ii} = C_T P_{ii}^T + C_L P_{ii}^L = \frac{\Pi_T}{1 - G_V\Pi_T} P_{ii}^T + \frac{\Pi_L}{1 - G_V\Pi_L} P_{ii}^L. \quad (4.15)$$

Using (4.11) and (4.12), it becomes for $D = 4$

$$\begin{aligned} C_{ii} &= \frac{\Pi_{ii} - \frac{\omega^2}{q^2}\Pi_{00}}{1 - \frac{G_V}{2}\left(\frac{\omega^2}{q^2}\Pi_{00} - \Pi_{ii}\right)} + \frac{\frac{\omega^2}{q^2}\Pi_{00}}{1 + G_V\left(\frac{Q^2}{q^2}\right)\Pi_{00}} \\ &= C'_T + C'_L. \end{aligned} \quad (4.16)$$

The imaginary part of the spatial vector correlator can be obtained as

$$\text{Im}C_{ii} = \text{Im}C'_T + \text{Im}C'_L. \quad (4.17)$$

where

$$\text{Im}C'_T = \frac{\text{Im}\Pi_{ii} - \frac{\omega^2}{q^2}\text{Im}\Pi_{00}}{\left[1 + \frac{G_V}{2}\text{Re}\Pi_{ii} - \frac{G_V}{2}\frac{\omega^2}{q^2}\text{Re}\Pi_{00}\right]^2 + \frac{G_V^2}{4}\left[\text{Im}\Pi_{ii} - \frac{\omega^2}{q^2}\text{Im}\Pi_{00}\right]^2}, \quad (4.18)$$

and,

$$\text{Im}C'_L = \frac{\frac{\omega^2}{q^2}\text{Im}\Pi_{00}}{\left[1 - G_V\left(1 - \frac{\omega^2}{q^2}\right)\text{Re}\Pi_{00}\right]^2 + \left[G_V\left(1 - \frac{\omega^2}{q^2}\right)\text{Im}\Pi_{00}\right]^2} = \frac{\omega^2}{q^2}\text{Im}C_{00}. \quad (4.19)$$

Following (2.5), the resummed vector spectral function

$$\sigma_V = \frac{1}{\pi}\left[\text{Im}C_{00} - \text{Im}C_{ii}\right]. \quad (4.20)$$

4.3 Conserved density fluctuation in ring approximation

Following (2.8) the response to the conserved density fluctuation, *i.e.*, QNS, at finite T and μ in ring approximation can be obtained in terms of the real part of the temporal correlation function C_{00} . The real part of C_{00} is obtained from (4.13) as

$$\text{Re}C_{00}(\omega, \vec{q}) = \frac{\text{Re}\Pi_{00}(\omega, \vec{q}) + G_V\left(\frac{\omega^2}{q^2} - 1\right)\left[(\text{Re}\Pi_{00}(\omega, \vec{q}))^2 + (\text{Im}\Pi_{00}(\omega, \vec{q}))^2\right]}{1 + 2G_V\left(\frac{\omega^2}{q^2} - 1\right)\text{Re}\Pi_{00}(\omega, \vec{q}) + \left(G_V\left(\frac{\omega^2}{q^2} - 1\right)\right)^2\left[(\text{Re}\Pi_{00}(\omega, \vec{q}))^2 + (\text{Im}\Pi_{00}(\omega, \vec{q}))^2\right]}. \quad (4.21)$$

Now the resummed QNS in ring approximation becomes

$$\chi_q^R(T, \tilde{\mu}) = -\lim_{\vec{q} \rightarrow 0} \text{Re}C_{00}(0, \vec{q}) = \frac{\chi_q(T, \tilde{\mu})}{1 + G_V\chi_q(T, \tilde{\mu})}, \quad (4.22)$$

where we note that $\lim_{\vec{q} \rightarrow 0} \text{Im}\Pi_{00}(0, \vec{q}) = 0$ and one-loop $\chi_q(T, \tilde{\mu}) = -\lim_{\vec{q} \rightarrow 0} \text{Re}\Pi_{00}(0, \vec{q})$.

Now, we note that at $G_V = 0$, all the resummed quantities in ring approximation become equivalent to those of one-loop. To compute all resummed quantities, we just need to compute one-loop vector self-energy within the effective models considered here.

4.4 Vector correlation function in one-loop

The current-current correlator in vector channel at one-loop level (refer figure 2) can be written as

$$\Pi_{\mu\nu}(Q) = \int \frac{d^4P}{(2\pi)^4} \text{Tr}_{D,c}[\gamma_\mu S(P+Q)\gamma_\nu S(P)], \quad (4.23)$$

where $\text{Tr}_{D,c}$ is trace over Dirac and color indices, respectively. We would like to compute this in effective models, *viz.*, in NJL and PNJL model.

The NJL quark propagator in Hartree approximation is given as

$$S_{\text{NJL}}(L) = [\not{L} - m_0 + \gamma_0\tilde{\mu} + G_S\sigma]^{-1} = [\not{L} - M_f + \gamma_0\tilde{\mu}]^{-1}, \quad (4.24)$$

whereas for PNJL it reads as

$$S_{\text{PNJL}}(L) = [\not{L} - M_f + \gamma_0\tilde{\mu} - i\gamma_0\mathcal{A}_4]^{-1} \quad (4.25)$$

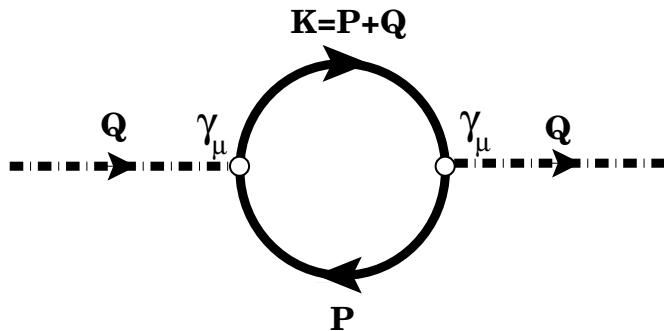


Figure 2. Vector channel correlator at one-loop.

where the four momentum, $L \equiv (l_0, \vec{l})$. The gap equation for constituent quark mass M_f and the modified quark chemical potential $\tilde{\mu}$ due to vector coupling G_V are given, respectively, in (3.3) and (3.4). Now in contrast to NJL one, the presence of background temporal gauge field \mathcal{A}_4 will make a connection to the Polyakov Loop field Φ [72–79]. While performing the frequency sum and color trace in (4.23), the thermal distribution function in PNJL case will be different from that of NJL one.

For convenience, we will calculate the one-loop vector correlation in NJL model. This NJL correlation function, as discussed, can easily be generalized to PNJL one by replacing the thermal distribution function² as

$$f(E_p \pm \tilde{\mu}) = \frac{\Phi e^{-\beta(E_p \pm \tilde{\mu})} + 2\bar{\Phi} e^{-2\beta(E_p \pm \tilde{\mu})} + e^{-3\beta(E_p \pm \tilde{\mu})}}{1 + 3\Phi e^{-\beta(E_p \pm \tilde{\mu})} + 3\bar{\Phi} e^{-2\beta(E_p \pm \tilde{\mu})} + e^{-3\beta(E_p \pm \tilde{\mu})}}, \quad (4.26)$$

which at $\Phi(\bar{\Phi}) = 1$ reduces to the thermal distribution for NJL or free as the cases may be. On the other hand for $\Phi(\bar{\Phi}) = 0$, the effect of confinement is clearly evident in which three quarks are stacked in a same momentum and color state [101].

4.4.1 Temporal part

The time-time component of the vector correlator in (4.23) reads as

$$\Pi_{00}(Q) = \int \frac{d^4 P}{(2\pi)^4} \text{Tr}[\gamma_0 S(K) \gamma_0 S(P)], \quad (4.27)$$

where $K = P + Q$. After some mathematical simplifications we are left with

$$\begin{aligned} \Pi_{00}(\omega, \vec{q}) = N_c N_f \int \frac{d^3 p}{(2\pi)^3} \frac{1}{E_p E_k} & \left\{ \frac{E_p E_k + M_f^2 + \vec{p} \cdot \vec{k}}{\omega + E_p - E_k} \right. \\ & \times [f(E_p - \tilde{\mu}) + f(E_p + \tilde{\mu}) - f(E_k - \tilde{\mu}) - f(E_k + \tilde{\mu})] \\ & + (E_p E_k - M_f^2 - \vec{p} \cdot \vec{k}) \left[\frac{1}{\omega - E_p - E_k} - \frac{1}{\omega + E_p + E_k} \right] \\ & \left. \times [1 - f(E_p + \tilde{\mu}) - f(E_k - \tilde{\mu})] \right\}. \end{aligned} \quad (4.28)$$

²For details we refer to refs. [84, 85].

The real and imaginary parts of the temporal vector correlator are, respectively, obtained as

$$\begin{aligned} \text{Re}\Pi_{00}(\omega, \vec{q}) = & \text{P} \left[N_f N_c \int \frac{d^3 p}{(2\pi)^3} \frac{1}{E_p E_k} \left\{ \frac{E_p E_k + M_f^2 + \vec{p} \cdot \vec{k}}{\omega + E_p - E_k} \right. \right. \\ & \times [f(E_p - \tilde{\mu}) + f(E_p + \tilde{\mu}) - f(E_k - \tilde{\mu}) - f(E_k + \tilde{\mu})] \\ & + (E_p E_k - M_f^2 - \vec{p} \cdot \vec{k}) \left(\frac{1}{\omega - E_p - E_k} - \frac{1}{\omega + E_p + E_k} \right) \\ & \left. \left. \times [1 - f(E_p + \tilde{\mu}) - f(E_k - \tilde{\mu})] \right\} \right], \end{aligned} \quad (4.29)$$

as P stands for principal value, and

$$\begin{aligned} \text{Im}\Pi_{00}(\omega, \vec{q}) = & \lim_{\eta \rightarrow 0} \frac{1}{2i} \left[\Pi_{00}(\omega \rightarrow \omega + i\eta, q) - \Pi_{00}(\omega \rightarrow \omega - i\eta, q) \right] \\ = & -\pi N_f N_c \int \frac{d^3 p}{(2\pi)^3} \frac{1}{E_p E_k} \left\{ (E_p E_k + M_f^2 + \vec{p} \cdot \vec{k}) \right. \\ & \times [f(E_p - \tilde{\mu}) + f(E_p + \tilde{\mu}) - f(E_k - \tilde{\mu}) - f(E_k + \tilde{\mu})] \times \delta(\omega + E_p - E_k) \\ & + (E_p E_k - M_f^2 - \vec{p} \cdot \vec{k}) [1 - f(E_p + \tilde{\mu}) - f(E_k - \tilde{\mu})] \\ & \left. \times [\delta(\omega - E_p - E_k)] \right\}. \end{aligned} \quad (4.30)$$

It is now worthwhile to check some known results in the limit $\vec{q} \rightarrow 0$ and $\tilde{\mu} = 0$, (4.30) can be written as:

$$\text{Im}\Pi_{00}(\omega) = -\pi N_f N_c \int \frac{d^3 p}{(2\pi)^3} \frac{1}{E_p^2} (3E_p^2 - 3M_f^2 - p^2) (2f'(E_p)) (-\omega \delta(\omega)), \quad (4.31)$$

and which, in the limit $M_f = m_0 - G_S \sigma = 0$, further becomes

$$\text{Im}\Pi_{00}(\omega) = -2\pi T^2 \omega \delta(\omega). \quad (4.32)$$

The vacuum part in (4.29) is now separated as

$$\begin{aligned} \text{Re}\Pi_{00}^{\text{vac}}(\omega, \vec{q}) = & \frac{N_f N_c}{4\pi^2} \int_0^\Lambda p dp \frac{1}{2E_p q} \left[4pq + 6E_p X_- - 6E_p X_+ - Y_- \ln \left| \frac{E_p + X_- - \omega}{E_p + X_+ - \omega} \right| \right. \\ & \left. + Y_+ \ln \frac{E_p + X_+ + \omega}{E_p + X_- + \omega} \right], \end{aligned} \quad (4.33)$$

$$\text{with } Y_\pm = (4E_p^2 \pm 4E_p \omega + M^2), \quad X_\pm = \sqrt{E_p^2 \pm 2pq + q^2} \quad \text{and} \quad M^2 = \omega^2 - q^2. \quad (4.34)$$

We note that the ultraviolet divergence in the vacuum part is regulated by using a finite three momentum cut-off Λ . The corresponding matter part of (4.29) is obtained as

$$\begin{aligned} \text{Re}\Pi_{00}^{\text{mat}}(\omega, \vec{q}) = & \frac{N_f N_c}{2\pi^2} \int_0^\infty p dp [f(E_p - \tilde{\mu}) + f(E_p + \tilde{\mu})] \left[\frac{\omega}{q} \ln \left| \frac{M^2 - 4(pq + \omega E_p)^2}{M^2 - 4(pq - \omega E_p)^2} \right| \right. \\ & \left. - \left(\frac{4E_p^2 + M^2}{4qE_p} \right) \ln \left| \frac{(M^2 - 2pq)^2 - 4\omega^2 E_p^2}{(M^2 + 2pq)^2 - 4\omega^2 E_p^2} \right| - \frac{2p}{E_p} \right]. \end{aligned} \quad (4.35)$$

The imaginary part in (4.30) can be simplified as

$$\text{Im}\Pi_{00}(\omega, \vec{q}) = \frac{N_f N_c}{4\pi} \int_{p_-}^{p_+} p \, dp \frac{4\omega E_p - 4E_p^2 - M^2}{2E_p q} [f(E_p - \tilde{\mu}) + f(E_p + \tilde{\mu}) - 1] \quad (4.36)$$

where the vacuum part does not require any momentum cut-off as the energy conserving δ -function ensures the finiteness of the limits:

$$p_{\pm} = \frac{\omega}{2} \sqrt{1 - \frac{4M_f^2}{M^2}} \pm \frac{q}{2}, \quad (4.37)$$

with a threshold restricted by a step function, $\Theta(M^2 - 4M_f^2)$.

4.4.2 Spatial part

The space-space component of the vector correlator in (4.23) reads as

$$\Pi_{ii}(Q) = \int \frac{d^4 P}{(2\pi)^4} \text{Tr}[\gamma_i S(K) \gamma_i S(P)], \quad (4.38)$$

which can be simplified to

$$\begin{aligned} \Pi_{ii}(\omega, \vec{q}) = N_c N_f \int \frac{d^3 p}{(2\pi)^3} \frac{1}{E_p E_k} & \left\{ \frac{3E_p E_k - 3M_f^2 - \vec{p} \cdot \vec{k}}{\omega - E_p + E_k} \right. \\ & \times [f(E_k + \tilde{\mu}) + f(E_k - \tilde{\mu}) - f(E_p + \tilde{\mu}) - f(E_p - \tilde{\mu})] \\ & + \left(3E_p E_k + 3M_f^2 + \vec{p} \cdot \vec{k} \right) \left[\frac{1}{\omega - E_p - E_k} - \frac{1}{\omega + E_p + E_k} \right] \\ & \left. \times [1 - f(E_k + \tilde{\mu}) - f(E_p - \tilde{\mu})] \right\}. \end{aligned} \quad (4.39)$$

In the similar way as before the imaginary part can be obtained

$$\begin{aligned} \text{Im}\Pi_{ii}(\omega, \vec{q}) = -\pi N_f N_c \int \frac{d^3 p}{(2\pi)^3} \frac{1}{E_p E_k} & \left\{ (3E_p E_k - 3M_f^2 - \vec{p} \cdot \vec{k}) \right. \\ & \times [f(E_k + \tilde{\mu}) + f(E_k - \tilde{\mu}) - f(E_p + \tilde{\mu}) - f(E_p - \tilde{\mu})] \delta(\omega + E_p - E_k) \\ & + \left(3E_p E_k + 3M_f^2 + \vec{p} \cdot \vec{k} \right) [1 - f(E_k + \tilde{\mu}) - f(E_p - \tilde{\mu})] \\ & \left. \times \delta(\omega - E_p - E_k) \right\}, \end{aligned} \quad (4.40)$$

whereas the real part can be obtained as

$$\begin{aligned} \text{Re}\Pi_{ii}(\omega, \vec{q}) = P \left[N_f N_c \int \frac{d^3 p}{(2\pi)^3} \frac{1}{E_p E_k} \right. & \left\{ \frac{3E_p E_k - 3M_f^2 - \vec{p} \cdot \vec{k}}{\omega - E_p + E_k} \right. \\ & \times [f(E_k - \tilde{\mu}) + f(E_k + \tilde{\mu}) - f(E_p - \tilde{\mu}) - f(E_p + \tilde{\mu})] \\ & + (3E_p E_k + 3M_f^2 + \vec{p} \cdot \vec{k}) \left(\frac{1}{\omega - E_p - E_k} - \frac{1}{\omega + E_p + E_k} \right) \\ & \left. \left. \times [1 - f(E_k + \tilde{\mu}) - f(E_p - \tilde{\mu})] \right\} \right]. \end{aligned} \quad (4.41)$$

At this point we also check the known results in the limit $\vec{q} \rightarrow 0$ and $\tilde{\mu} = 0$, (4.40) can be written as:

$$\begin{aligned} \text{Im}\Pi_{ii}(\omega) &= -\pi N_f N_c \int \frac{d^3p}{(2\pi)^3} \frac{1}{E_p^2} (3E_p^2 - 3M_f^2 - p^2) (2f'(E_p)) (-\omega\delta(\omega)) \\ &\quad - \frac{3}{2\pi\omega} \sqrt{\omega^2 - 4M_f^2} (\omega^2 + 2M_f^2) \tanh\left(\frac{\omega}{4T}\right) \Theta(\omega - 2M_f), \end{aligned} \quad (4.42)$$

and when $M_f = m_0 - G_S\sigma = 0$, it becomes

$$\text{Im}\Pi_{ii}(\omega) = -2\pi T^2 \omega \delta(\omega) - \frac{3}{2\pi} \omega^2 \tanh\left(\frac{\omega}{4T}\right). \quad (4.43)$$

As seen both massive and massless cases show a sharp peak due to the delta function at $\omega \rightarrow 0$, which leads to pinch singularity for calculation of transport coefficients.

Now, the vacuum part in (4.41) is simplified as

$$\begin{aligned} \text{Re}\Pi_{ii}^{\text{vac}}(\omega, \vec{q}) &= \frac{N_f N_c}{4\pi^2} \int_0^\Lambda p dp \frac{1}{2E_p q} \left[-4pq + 10E_p(X_- - X_+) - Z_- \ln \left| \frac{E_p + X_- - \omega}{E_p + X_+ - \omega} \right| \right. \\ &\quad \left. + Z_+ \ln \frac{E_p + X_+ + \omega}{E_p + X_- + \omega} \right], \end{aligned} \quad (4.44)$$

where $Z_\pm = 4p^2 \pm 4E_p\omega - M^2$. The corresponding matter part is obtained as

$$\begin{aligned} \text{Re}\Pi_{ii}^{\text{mat}}(\omega, \vec{q}) &= \frac{N_f N_c}{4\pi^2} \int_0^\infty p dp [f(E_p - \tilde{\mu}) + f(E_p + \tilde{\mu})] \left[2\frac{\omega}{q} \ln \left| \frac{M^2 - 4(pq + E_p\omega)^2}{M^2 - 4(pq - E_p\omega)^2} \right| \right. \\ &\quad \left. + \left(\frac{M^2 - 4p^2}{2qE_p} \right) \ln \left| \frac{(M^2 - 2pq)^2 - 4\omega^2 E_p^2}{(M^2 + 2pq)^2 - 4\omega^2 E_p^2} \right| + 4\frac{p}{E_p} \right]. \end{aligned} \quad (4.45)$$

Finally, the imaginary part in (4.40) is simplified as

$$\text{Im}\Pi_{ii}(\omega, \vec{q}) = \frac{N_f N_c}{4\pi} \int_{p_-}^{p_+} p dp \frac{4\omega E_p - 4p^2 + M^2}{2E_p q} (f(E_p - \tilde{\mu}) + f(E_p + \tilde{\mu}) - 1) \quad (4.46)$$

where the vacuum part does not need any finite momentum cut-off as stated above.

5 Results

5.1 Gap equations and mean fields

The thermodynamic potential Ω for both NJL and PNJL model is extremized with respect to the mean fields X , i.e.,

$$\frac{\partial \Omega}{\partial X} = 0 \quad (5.1)$$

where, X stands for σ and n for NJL model and $\Phi, \bar{\Phi}, \sigma$ and n for PNJL model. The value of the parameters, $G_S = 10.08 \text{ GeV}^{-2}$ and $\Lambda = 0.651 \text{ GeV}$ were taken from literature [83] and $m_0 = 0.005 \text{ GeV}$. However, the value of G_V is difficult to fix within the model formalism, since this quantity should be fixed using the ρ meson mass which, in general, happens to be

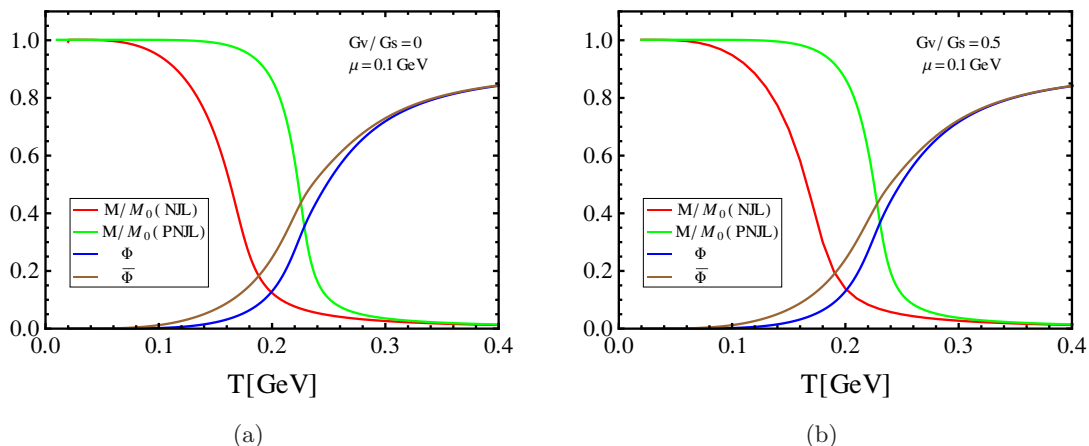


Figure 3. Variation of scaled constituent quark mass with zero temperature quark mass and the Polyakov Loop fields (Φ and $\bar{\Phi}$) with temperature at chemical potential $\mu = 100$ MeV for (a) $G_V/G_S = 0$ and (b) $G_V/G_S = 0.5$.

higher than the maximum energy scale Λ of the model. So, we consider the vector coupling constant G_V as a free parameter and different choices are considered as $G_V = x \times G_S$, where x is chosen from 0 to 1 appropriately.

In figure 3 a comparison between the scaled quark mass with its zero temperature value ($M_f(T)/M_f(0)$) in NJL and PNJL model is displayed as a function of temperature T for two values of $G_V (= 0 \text{ and } 0.5G_S)$ with $\mu = 100$ MeV. It also contains a variation of the Polyakov loop fields ($\Phi(T)$ and $\bar{\Phi}(T)$) with T . In both models the scaled quark mass decreases with increase in T and approaches the chiral limit at very high T . However, in the temperature range $60 \leq T(\text{MeV}) \leq 300$, the variation of the scaled quark mass is slower in PNJL than that of NJL model. This slow variation is due to the presence of the confinement effect in it through the Polyakov Loop fields ($\Phi(T)$ and $\bar{\Phi}(T)$), as can be seen that the Polyakov Loop field ($\Phi(T)$) and its conjugate ($\bar{\Phi}(T)$) increase from zero in confined phase and approaches unity (free state) at high temperature. Now, we note that $\Phi = \bar{\Phi}$ at $\mu = 0$ as there is equal number of quarks and antiquarks. However, because of non-zero chemical potential there is an asymmetry in quark and antiquark numbers, which leads to an asymmetry in the Polyakov Loop fields Φ and $\bar{\Phi}$. This asymmetry disappears for $T > 300$ MeV, which is much greater than μ . We also note that the fields depend weakly with the variation of the vector coupling G_V akin to that of mass as displayed in figure 4 for $\mu = 100$ MeV and $G_V/G_S = 0$ to 0.8.

In figure 5 the number density scaled with T^3 for both NJL and PNJL model is displayed as a function of T with $\mu = 100$ MeV for two values of G_V . At very high temperature, as seen in figure 3, the Polyakov Loop fields $\Phi(\bar{\Phi}) \rightarrow 1$ and masses in both models become same. So, PNJL model becomes equivalent to NJL model because the thermal distribution function becomes equal as can be seen from (4.26) and thus the number density. On the other hand, for temperature $T < 400$ MeV and a given μ , the PNJL number density is found to be suppressed than that of NJL case as the thermal distribution function in (4.26) is suppressed. This is due to the combination of two complementary effects:

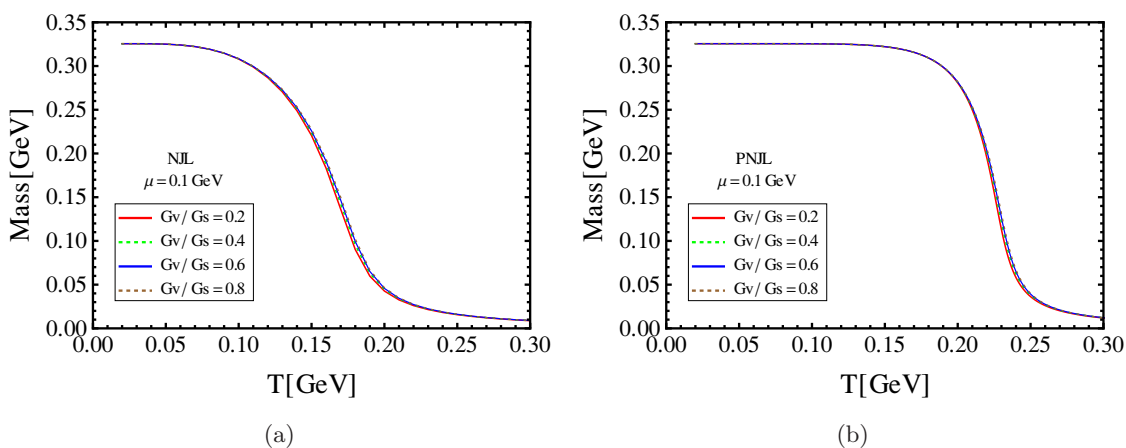


Figure 4. Variation of constituent quark mass with temperature in (a) NJL and (b) PNJL model for chemical potential $\mu = 100$ MeV and a set of values for vector coupling G_V .

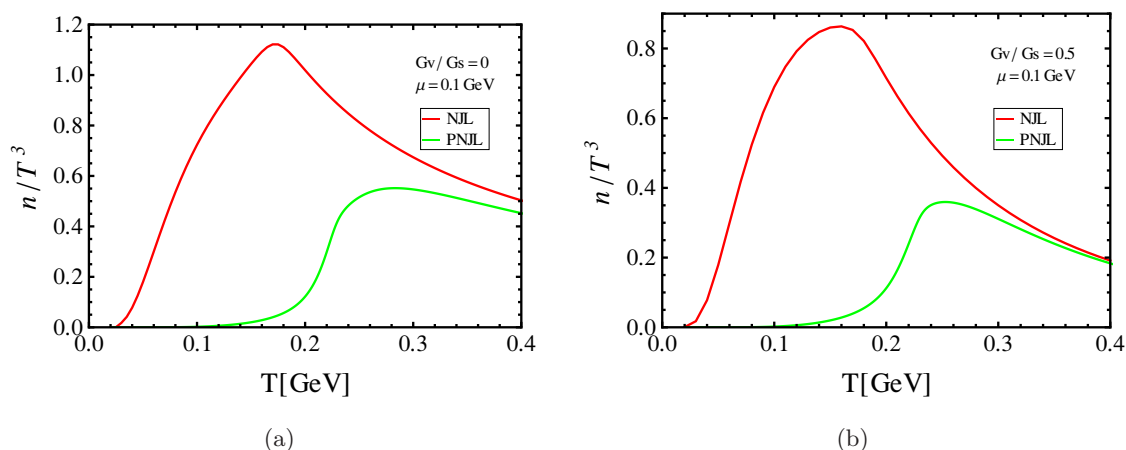


Figure 5. Comparison of the scaled quark number density with T^3 as a function of T in NJL and PNJL model with chemical potential $\mu = 100$ MeV for (a) $G_V/G_S = 0$ and (b) $G_V/G_S = 0.5$.

(i) the nonperturbative effect through Φ and $\bar{\Phi}$ and (ii) the slower variation of mass in PNJL model, which are clearly evident from figure 3. It is also obvious from figure 5(a) and figure 5(b) that the presence of vector interaction G_V reduces the number density for both NJL and PNJL model, which could be understood due to the reduction of $\tilde{\mu}$ as given in (3.4).

5.2 Vector spectral function and dilepton rate

The vector spectral function is proportional to the imaginary part of the vector correlation function as defined in (2.5) or (4.20). This imaginary part is restricted by, the energy conservation, $\omega = E_p + E_k$, as can be seen from (4.30) and (4.40). This equivalently leads to a threshold, $M^2 \geq 4M_f^2$, which can also be found from (4.37). Now for a given G_V and T , the resummed spectral function in (4.20) picks up continuous contribution above the

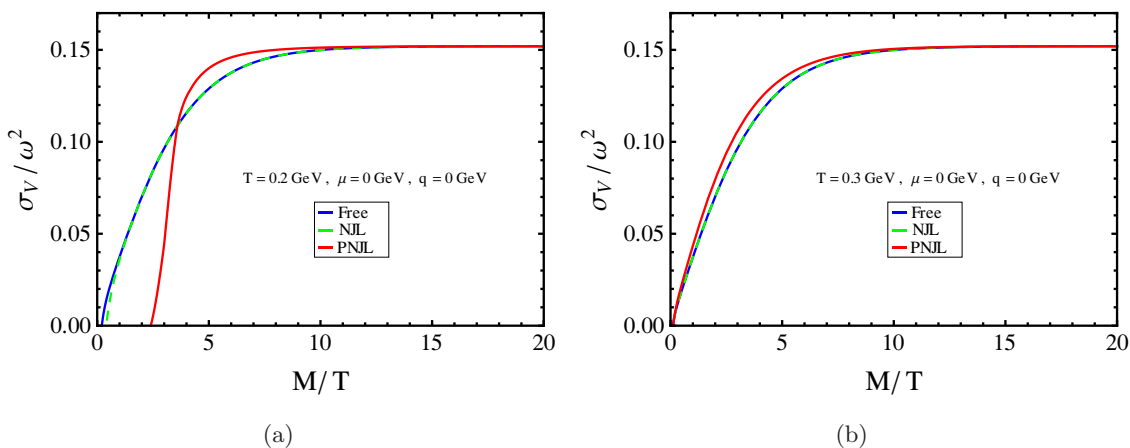


Figure 6. Scaled vector spectral function σ_V/ω^2 as a function of scaled invariant mass, M/T , in NJL and PNJL model with external momentum $q = 0$, quark chemical potential $\mu = 0$ and $G_V/G_S = 0$ for (a) $T = 200$ MeV and (b) $T = 300$ MeV.

threshold, $M^2 > 4M_f^2$, which provides a finite width to a vector meson that decays into a pair of leptons. However, below the threshold $M^2 < 4M_f^2$, the continuous contribution of the spectral function in (4.20) becomes zero and the decay to dileptons are forbidden. But if one analyses it below the threshold, one can find bound state contributions in spectral functions. When imaginary part approaches zero, the spectral function in (4.20) becomes discrete and can be written as:

$$\sigma_V(\omega, \vec{q}) \stackrel{M < 2M_f}{=} \frac{1}{\pi} \left[\delta(F_1(\omega, \vec{q})) \right],$$

$$\text{where } F_1(\omega, \vec{q}) = 1 + \frac{G_V}{2} \text{Re}\Pi_{ii} - \frac{G_V}{2} \frac{\omega^2}{q^2} \text{Re}\Pi_{00} = 0, \tag{5.2}$$

where only the dominant contribution of (4.18) is considered. Using the properties of δ -function, one can write

$$\sigma_V(\omega, \vec{q}) \stackrel{M < 2M_f}{=} \frac{1}{\pi} \frac{\delta(\omega - \omega_0)}{|dF_1(\omega, \vec{q})/d\omega|_{\omega=\omega_0}}, \tag{5.3}$$

which corresponds to a sharp δ -function peak at $\omega = \omega_0$. However, we are interested here in continuous contribution $M > 2M_f$, which are discussed below.

5.2.1 Without vector interaction ($G_V = 0$)

With no vector interaction ($G_V = 0$), the spectral function in (4.20) is solely determined by the imaginary part of the one loop vector self energies $\Pi_{00}(\omega, \vec{q})$ and $\Pi_{ii}(\omega, \vec{q})$. Figure 6 displays a comparison of vector spectral function with zero external momentum ($\vec{q} = 0, M = \omega$) in NJL and PNJL model for $T = 200$ MeV and 300 MeV, when there is no vector interaction ($G_V = 0$). Now, for $T = 200$ MeV (left panel) the spectral function in PNJL model has larger threshold than NJL model because the quark mass in PNJL model is much larger than that of NJL one (see figure 3). Also the PNJL spectral function

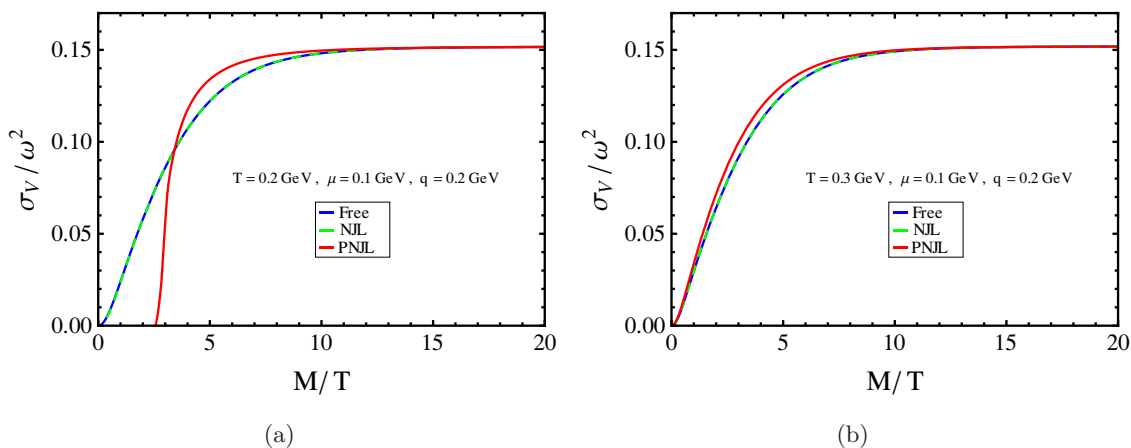


Figure 7. Scaled vector spectral function σ_V/ω^2 as a function of scaled invariant mass, M/T , in NJL and PNJL model with external momentum $q = 200$ MeV, quark chemical potential $\mu = 100$ MeV and $G_V/G_S = 0$ for (a) $T = 200$ MeV and (b) $T = 300$ MeV.

dominates over that of NJL one, because of the presence of nonperturbative effects due to Polyakov Loop fields Φ and $\bar{\Phi}$. At higher values of T ($= 300$ MeV) (right panel), the threshold becomes almost same due to the reduction of mass effect in PNJL case whereas the nonperturbative effects at low M/T still dominate. The reason is the following: at zero external momentum and zero chemical potential the spectral function is proportional to $[1 - 2f(E_p)]$ (apart from the mass dependent prefactor) as can be seen from the second term of (4.42). In PNJL case the thermal distribution function, $f(E_p)$, is more suppressed due to the suppression of color degrees of freedom than NJL at moderate values of T , so the weight factor $[1 - 2f(E_p)]$ is larger than NJL case and causing an enhancement in the spectral function. All these features also persist at non-zero chemical potential and external momentum as can also be seen from figure 7.

At this point it is important to note that for $T > 250$ MeV the mass in NJL model almost approaches current quark mass (see figure 3(a)) and can be considered as a free case since there is no vector interaction present ($G_V = 0$). Nevertheless, the PNJL case is different because of the presence of the nonperturbative confinement effect through the Polyakov Loop fields. The PNJL model can suitably describe a semi-QGP [70, 71, 103] scenario having nonperturbative effect due to the suppression of color degrees of freedom compared to NJL vis-a-vis free case above the deconfinement temperature.

The above features of the spectral function in a semi-QGP with no vector interaction will be reflected in the dilepton rate which is related to the spectral function, as given in (2.7). In figure 8, the dilepton rate is displayed as a function of scaled invariant mass M with T . As already discussed, at this temperatures the quark mass in NJL approaches current quark mass faster than PNJL, thus the dilepton rates for Born and NJL cases become almost the same. However, the dilepton rate in PNJL model is enhanced than those of Born or NJL case. This in turn suggests that the nonperturbative dilepton production rate is higher in a semi-QGP than the Born rate in a weakly coupled QGP. The dilepton rate is also compared with that from LQCD result [35] within a quenched approximation.

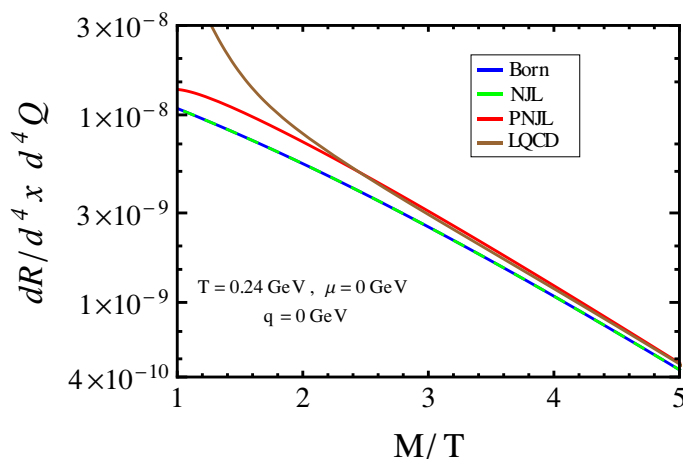


Figure 8. Comparison of dilepton rates as a function of M/T for $T = 240$ MeV with external momentum $q = 0$, quark chemical potential $\mu = 0$ and $G_V/G_S = 0$. The LQCD rate is from ref. [35].

It is found to agree well for $M/T \geq 2$, below which it differs from LQCD rate. We try to understand this as follows: the spectral function in LQCD is extracted using MEM from Euclidean vector correlation function by inverting (2.6), which requires an ansatz for the spectral function. Using a free field spectral function as an ansatz, the spectral function in a quenched approximation of QCD was obtained earlier [43] by inverting (2.6), which was then approaching zero in the limit $M/T \rightarrow 0$. So was the first lattice dilepton rate [43] at low M/T whereas it was oscillating around the Born rate for $M/T > 3$. Now, in a very recent LQCD calculation [35] with larger size, while extracting the spectral function using MEM from Euclidean vector correlation function, an ansatz for the spectral function, a Briet-Wigner (BW) for low M/T plus a free field one for $M/T \geq 2$, has been used. The ansatz of BW at low M/T pushes up the spectral function and so is the recent dilepton rate in LQCD below $M/T \leq 2$. However, no such ansatz is required in thermal QCD and we can directly calculate the spectral function without any uncertainty by virtue of the analytic continuation.

In figure 9 the dilepton rate is also displayed at $T = 300$ MeV, non-zero chemical potential ($\mu = 100$ MeV) and external momentum ($q = 0$ and 200 MeV). We note that this information could also be indicative for future LQCD computation of dilepton rate at non-zero μ and q . The similar feature of semi-QGP as found in figure 8 is also seen here but with a quantitative difference especially due to higher T , which could be understood from figure 3(a).

5.2.2 With vector interaction ($G_V \neq 0$)

In figure 10 the spectral function for $G_V/G_S = 0.5$ with $q = 200$ MeV and $\mu = 100$ MeV in NJL (left panel) and PNJL (right panel) model is displayed. At $T = 100 < T_c \sim 160$ MeV [101, 104–106] the spectral function above the respective threshold, $M > 2M_f$, starts with a large value because the denominator in (4.18) is very small compared to those

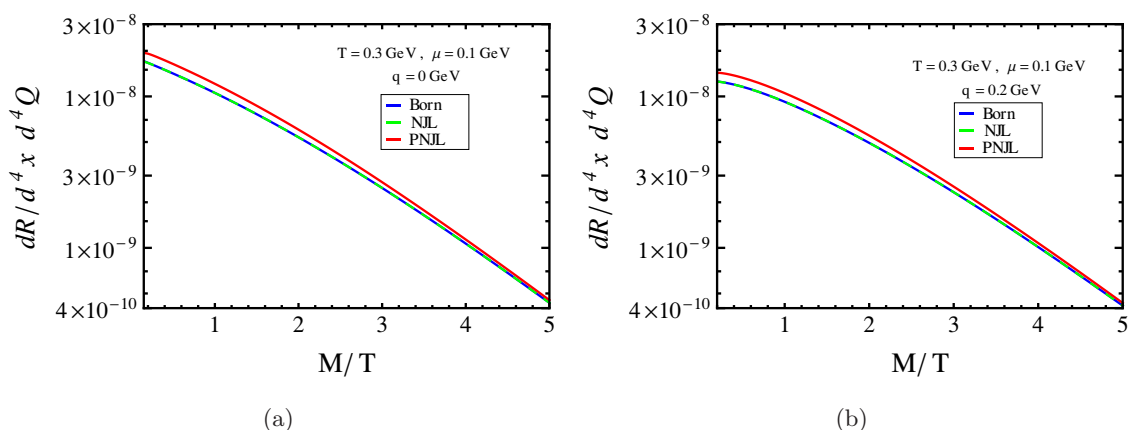


Figure 9. Different dilepton rates as a function of M/T at $T = 300$ MeV, $\mu = 100$ MeV and $G_V/G_S = 0$ for (a) $q = 0$ (b) $q = 200$ MeV.

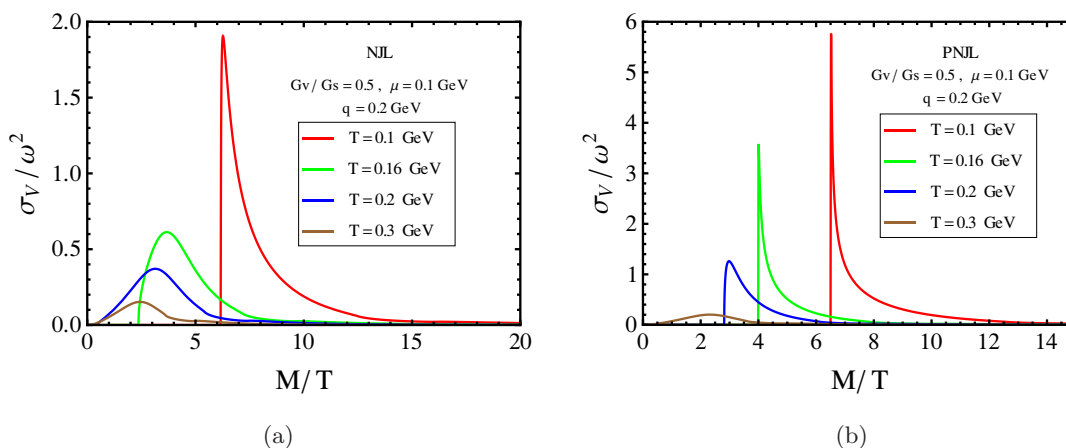


Figure 10. Scaled spectral function as a function of M/T in (a) NJL and (b) PNJL model for a set of T with $\mu = 100$ MeV, $q = 200$ MeV and $G_V/G_S = 0.5$. Note the difference in y -scale.

in (4.14) and (4.19). This is due to the two reasons: (i) the first term in the denominator involving real parts of Π has zero below the threshold that corresponds to a sharp δ -like peak as discussed in (5.3), thus it also becomes a very small number just above the threshold and (ii) the second term involving imaginary parts start building up, which is also very small. However, the increase in T causes the spectral function to decrease due to mutual effects of denominator (involving both real and imaginary parts of Π) and numerator (involving only imaginary parts of Π). On the other hand, with the increase in T , the threshold in NJL case reduces quickly as the quark mass decreases faster whereas it reduces slowly for PNJL case because the Polyakov Loop fields experience a slow variation of the quark mass. So, the vector meson in NJL model acquires a width earlier than the PNJL model due to suppression of color degrees of freedom in presence of Polyakov Loop fields. As seen, for NJL model at $T = T_c \sim 160$ MeV the sharp peak like structure gets a substantial width

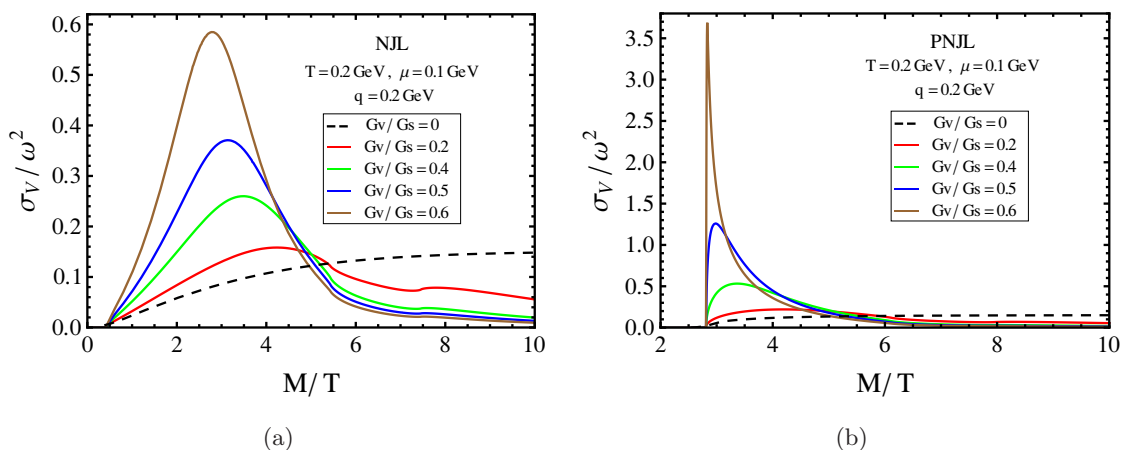


Figure 11. Scaled spectral function as a function of M/T for (a) NJL and (b) PNJL model with $T = 200 \text{ MeV}$, $\mu = 100 \text{ MeV}$, $q = 200 \text{ MeV}$ and a set of values of $G_V/G_S = 0, 0.2, 0.4, 0.5$ and 0.6 .

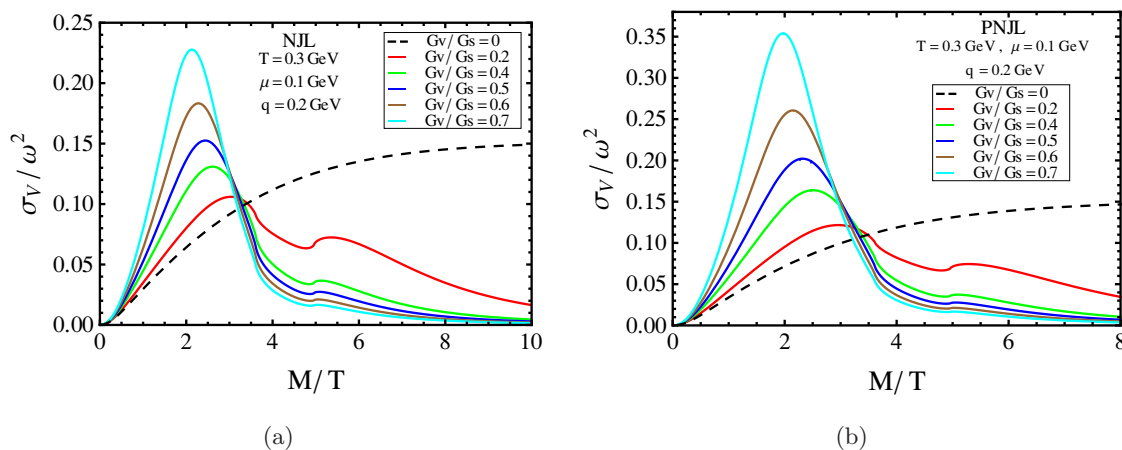


Figure 12. Scaled spectral function as a function of M/T for (a) NJL and (b) PNJL model with $T = 300 \text{ MeV}$, $\mu = 100 \text{ MeV}$, $q = 200 \text{ MeV}$ and a set of values of $G_V/G_S = 0, 0.2, 0.4, 0.5, 0.6$ and 0.7 .

than PNJL model. This suggests that the vector meson retains its bound properties at and above T_c in PNJL model in presence of G_V along with the nonperturbative effects through Polyakov Loop fields.

In figures 11 and 12 we present the dependence of the spectral function on the vector interaction in QGP for a set of values of the coupling G_V in NJL (left panel) and PNJL (right panel) model, respectively, for $T = 200$ and $T = 300 \text{ MeV}$. In both cases the spectral strength increases with that of G_V . Nevertheless, the strength of the spectral function in PNJL case at a given T and G_V is always stronger than that of NJL model. This suggests that the presence of the vector interaction further suppresses the color degrees of freedom in addition to the Polyakov Loop fields. The dilepton rates corresponding to $T = 300 \text{ MeV}$ are also displayed in figure 13, which show an enhancement at low M/T compared to

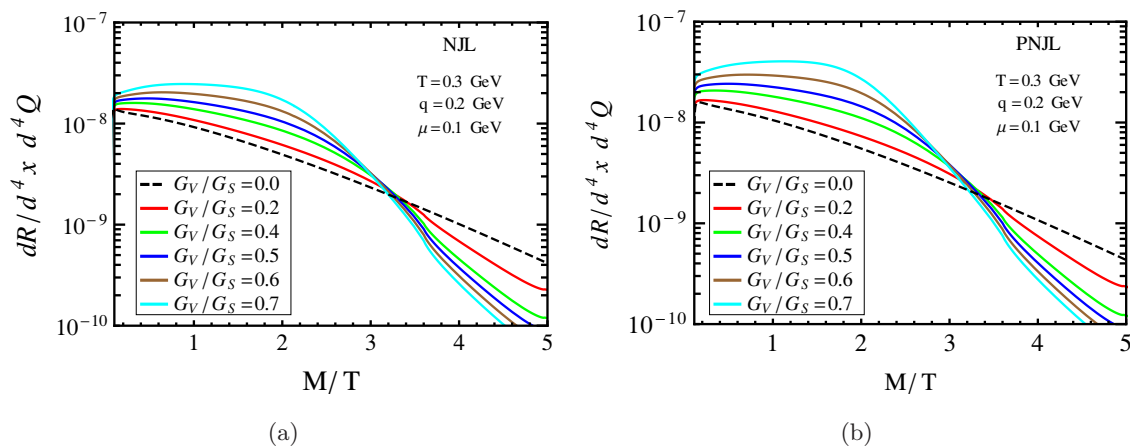


Figure 13. Dilepton rates as a function of M/T (a) NJL and (b) PNJL model for a set of values of G_V/G_S with $T = 300$ MeV with external momentum $q = 200$ MeV, quark chemical potential $\mu = 100$ MeV.

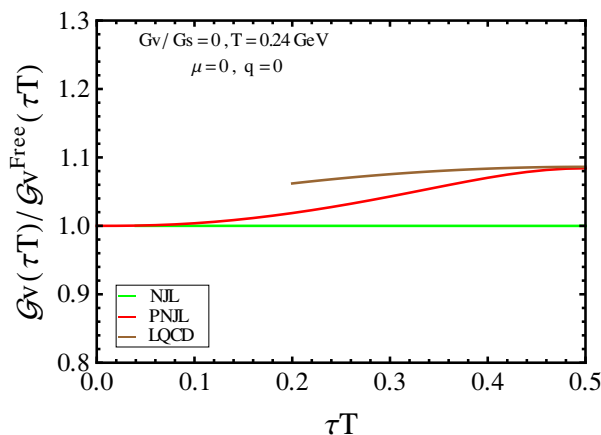


Figure 14. Comparison of various scaled Euclidean correlation function with respect to that of free field theory, $\mathcal{G}_V(\tau T)/\mathcal{G}_V^{\text{free}}(\tau T)$, as a function of the scaled Euclidean time τT for $T = 240$ MeV with external momentum $q = 0$, quark chemical potential $\mu = 0$ and $G_V/G_S = 0$. The continuum extrapolated LQCD result is from ref. [35].

$G_V = 0$ case. The enhancement in PNJL case indicates that more lepton pairs will be produced at low mass ($M/T < 4$) in semi-QGP with vector interaction, which would be appropriate for the hot and dense matter likely to be produced at FAIR energies.

5.3 Vector correlation function

The vector correlation function can be obtained using (2.6) in the scaled Euclidean time $\tau T \in [0, 1]$. We note that the correlation function in the τT range is symmetrical around $\tau T = 1/2$ due to the periodicity condition in Euclidean time guaranteed by the kernel $\cosh[\omega(2\tau T - 1)/2T]/\sinh(\omega/2T)$ in (2.6).

In figure 14 a comparison of the ratio of the vector correlation function to that of free one is displayed at $T = 240$ MeV, $G_V/G_S = 0$, $\mu = 0$ and $q = 0$ for NJL, PNJL and the

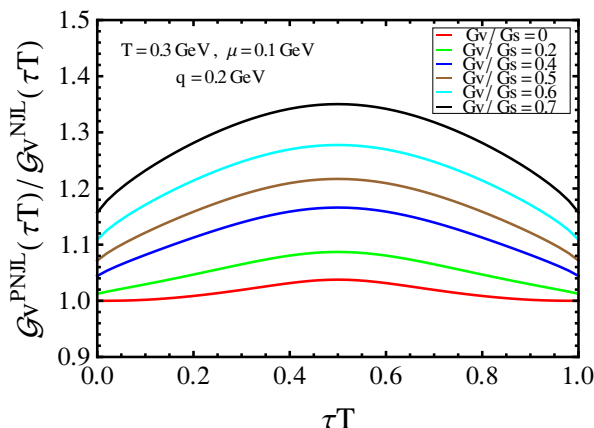


Figure 15. Ratio of Euclidean correlation function in PNJL model to that of NJL model as a function of τT at $T = 300$ MeV, $\mu = 100$ MeV and $q = 200$ MeV with a set of values of G_V/G_S .

continuum extrapolated LQCD data [35] in quenched approximation. It is plotted in the τT range $[0, 1/2]$ because LQCD data are available for the same range. As seen the NJL case becomes equal to that of free one as there is no effects from background gauge fields. On the other hand the PNJL result at $\tau T = 0$ and 1 becomes similar to those of free case because $\sigma_V^{\text{PNJL}}(\omega)/\sigma_V^{\text{free}}(\omega) = 1$ as $\omega \rightarrow \infty$. Around $\tau T = 1/2$ it deviates maximum from the free case due to the difference in spectral function at small ω and thus a nontrivial correlation exists among color charges due to the presence of the nonperturbative Polyakov Loop fields. This features are consistent with those in the spectral function in figure 6 and the dilepton rate in figure 8. In contrary, the correlation function around $\tau T = 1/2$ agrees better with that of LQCD in quenched approximation [35].

In figure 15, we display the effect of the vector interaction G_V in addition to the presence of the Polyakov Loop fields in QGP through the ratio of the correlation function in PNJL model to that of NJL model. Here we have displayed the result in the full range of the scaled Euclidean time $\tau T \in [0, 1]$. As discussed the ratio is symmetric around $\tau T = 1/2$ and always stay above unity. The ratio increases with the increase of the strength of the vector interaction. This is due to the fact that PNJL correlation function is always larger than that of the NJL case since $\sigma_V^{\text{PNJL}}(\omega, \vec{q})/\sigma_V^{\text{NJL}}(\omega, \vec{q}) > 1$, and it is even stronger in particular at small ω (see figure 12). This indicates that the color charges maintain a strong correlation among them due to the presence of both Polyakov Loop fields and the vector interaction. Thus the vector meson retains its bound properties in the deconfined phase.

5.4 Quark number susceptibility and temporal correlation function

Now, we can calculate quark number susceptibility (QNS) associated with the temporal part of the vector spectral function through the conserved density fluctuation as given in (4.22). The resummed susceptibility for a set of values of G_V at finite quark chemical potential ($\mu = 100$ MeV) is shown in figure 16. For positive vector coupling G_V the denominator of (4.22) is always greater than unity and as a result the resummed susceptibility gets suppressed as one increases G_V . Since positive G_V implies a repulsive interaction,

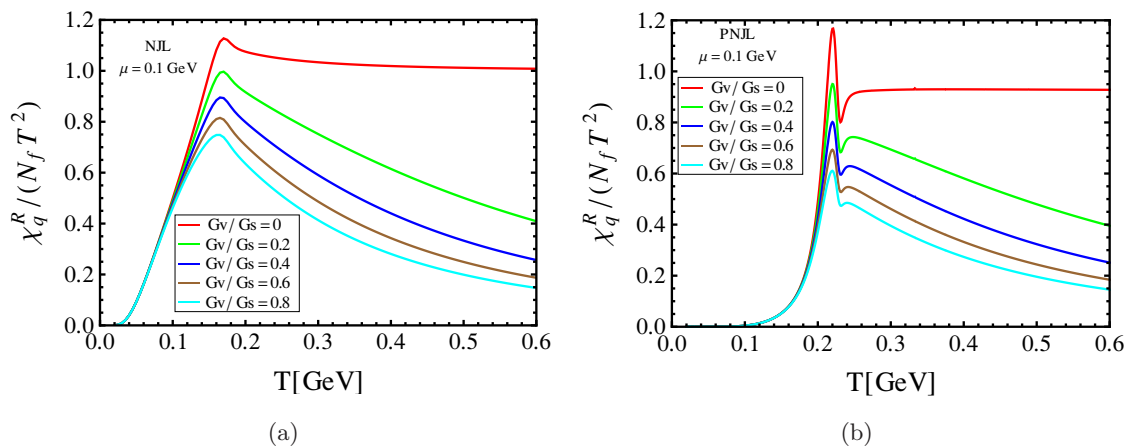


Figure 16. Resummed quark number susceptibility in (a) NJL model and (b) PNJL model at non-zero chemical potential for two flavor ($N_f = 2$).

the compressibility of the system decreases with increase of G_V , hence the susceptibility as seen from figure 16 decreases. We note that the QNS at finite μ shows an important feature around the phase transition temperature than that at $\mu = 0$ [84]. This is due to the fact that the mean fields ($X = \sigma$, Φ and $\bar{\Phi}$) which implicitly depend on μ contributes strongly as the change of these fields are most significant around the transition region. This feature could be important in the perspective of FAIR scenario where a hot but very dense matter is expected to be created. Using (2.10) one can compute the temporal Euclidean correlation function associated with the QNS as $\mathcal{G}_{00}^E(\tau T)/T = -\chi_q^R(T)$, which does not depend on τ but on T . This study could also provide useful information to future LQCD calculation at finite μ .

6 Conclusion

In the present work, the behavior of the vector meson correlation function and its spectral representation, and various physical quantities associated with the spectral representation, in a hot and dense environment, have been studied within the effective model framework, *viz.* NJL and PNJL model. PNJL model contains additional nonperturbative information through Polyakov Loop fields than NJL model. In addition to this nonperturbative effect of Polyakov Loop, the repulsive isoscalar-vector interaction is also considered. The influence of such interaction on the correlator and its spectral representation in a hot and dense medium has been obtained using ring resummation known as Random Phase Approximation. The incorporation of vector interaction is important, in particular, for various spectral properties of the system at non-zero chemical potential. However, the value of the vector coupling strength is difficult to fix from the mass scale which is higher than the maximum energy scale Λ of the effective theory. So, we have made different choices of this vector coupling strength to understand qualitatively its effect on the various quantities we have computed.

In absence of the isoscalar-vector interaction, the static spectral function and the correlation function in NJL model become quantitatively equivalent to those of free field theory. In case of PNJL these quantities are different from both free and NJL case because of the

presence of the nonperturbative Polyakov Loop fields that suppress the color degrees of freedom in the deconfined phase just above T_c . This suggests that some nontrivial correlation exist among the color charges in the deconfined phase. As an important consequence, the nonperturbative dilepton production rate is enhanced in the deconfined phase compared to the leading order perturbative rate. We note that the Euclidean correlation function and the nonperturbative rate with zero chemical potential agree well with the available LQCD data in quenched approximation. We also discussed these quantities in presence of finite chemical potential and external momentum which could provide useful information if, in future, LQCD computes them at finite chemical potential and external momentum.

In presence of the isoscalar-vector interaction, appropriate for hot but very dense medium likely to be created at FAIR GSI, it is found that the color degrees of freedoms are, further, suppressed up to a moderate value of the temperature above the critical temperature implying a stronger correlation among the color charges in the deconfined phase. The correlation function, spectral function and its spectral property, e.g., the low mass dilepton rate are strongly affected in PNJL case than NJL case. We also note that the response to the conserved number density fluctuation at finite chemical potential exhibits an interesting characteristic around the phase transition temperature than that at vanishing chemical potential. This is because the mean fields (Polyakov Loop fields and condensates etc.) depend implicitly on chemical potential and so their variations are most significant around the transition region, in particular for PNJL model. Finally, some of our results presented in this work can be tested when LQCD computes them, in future, with the inclusion of the dynamical fermions.

Acknowledgments

CAI would like to acknowledge the financial support from the University Grants Commission, India. SM, NH and MGM acknowledge the Department of Atomic Energy, India for the financial support through the project name TPAES. SM would like to thank Anirban Lahiri for useful discussions. Finally, we would also like to acknowledge very useful discussions and comments we had with Purnendu Chakraborty and Aritra Bandyopadhyay during this work.

Open Access. This article is distributed under the terms of the Creative Commons Attribution License ([CC-BY 4.0](https://creativecommons.org/licenses/by/4.0/)), which permits any use, distribution and reproduction in any medium, provided the original author(s) and source are credited.

References

- [1] B. Muller, *The Physics Of The Quark-Gluon Plasma*, *Lect. Notes Phys.* **225** (1985) 1.
- [2] U.W. Heinz and M. Jacob, *Evidence for a new state of matter: An Assessment of the results from the CERN lead beam program*, [nucl-th/0002042](#) [[INSPIRE](#)].
- [3] BRAHMS collaboration, I. Arsene et al., *Quark gluon plasma and color glass condensate at RHIC? The Perspective from the BRAHMS experiment*, *Nucl. Phys. A* **757** (2005) 1 [[nucl-ex/0410020](#)] [[INSPIRE](#)].

- [4] B.B. Back et al., *The PHOBOS perspective on discoveries at RHIC*, *Nucl. Phys. A* **757** (2005) 28 [[nucl-ex/0410022](#)] [[INSPIRE](#)].
- [5] STAR collaboration, J. Adams et al., *Experimental and theoretical challenges in the search for the quark gluon plasma: The STAR Collaboration's critical assessment of the evidence from RHIC collisions*, *Nucl. Phys. A* **757** (2005) 102 [[nucl-ex/0501009](#)] [[INSPIRE](#)].
- [6] PHENIX collaboration, K. Adcox et al., *Formation of dense partonic matter in relativistic nucleus-nucleus collisions at RHIC: Experimental evaluation by the PHENIX collaboration*, *Nucl. Phys. A* **757** (2005) 184 [[nucl-ex/0410003](#)] [[INSPIRE](#)].
- [7] ALICE collaboration, *ALICE: Physics performance report, volume I*, *J. Phys. G* **30** (2004) 1517 [[INSPIRE](#)].
- [8] ALICE collaboration, *ALICE: Physics performance report, volume II*, *J. Phys. G* **32** (2006) 1295 [[INSPIRE](#)].
- [9] B. Friman et al., *The CBM physics book: Compressed baryonic matter in laboratory experiments*, *Lect. Notes Phys.* **814** (2011) 1.
- [10] PHENIX collaboration, A. Adare et al., *Detailed measurement of the e^+e^- pair continuum in $p+p$ and $Au+Au$ collisions at $\sqrt{s_{NN}} = 200$ GeV and implications for direct photon production*, *Phys. Rev. C* **81** (2010) 034911 [[arXiv:0912.0244](#)] [[INSPIRE](#)].
- [11] PHENIX collaboration, S.S. Adler et al., *Measurement of direct photon production in $p+p$ collisions at $\sqrt{s} = 200$ GeV*, *Phys. Rev. Lett.* **98** (2007) 012002 [[hep-ex/0609031](#)] [[INSPIRE](#)].
- [12] PHENIX collaboration, A. Adare et al., *Scaling properties of azimuthal anisotropy in $Au+Au$ and $Cu+Cu$ collisions at $\sqrt{s_{NN}} = 200$ GeV*, *Phys. Rev. Lett.* **98** (2007) 162301 [[nucl-ex/0608033](#)] [[INSPIRE](#)].
- [13] PHENIX collaboration, K. Adcox et al., *Suppression of hadrons with large transverse momentum in central $Au+Au$ collisions at $\sqrt{s_{NN}} = 130$ GeV*, *Phys. Rev. Lett.* **88** (2002) 022301 [[nucl-ex/0109003](#)] [[INSPIRE](#)].
- [14] PHENIX collaboration, K. Adcox et al., *Measurement of the Lambda and anti-Lambda particles in $Au+Au$ collisions at $\sqrt{s_{NN}} = 130$ GeV*, *Phys. Rev. Lett.* **89** (2002) 092302 [[nucl-ex/0204007](#)] [[INSPIRE](#)].
- [15] PHENIX collaboration, S.S. Adler et al., *Scaling properties of proton and anti-proton production in $\sqrt{s_{NN}} = 200$ GeV $Au+Au$ collisions*, *Phys. Rev. Lett.* **91** (2003) 172301 [[nucl-ex/0305036](#)] [[INSPIRE](#)].
- [16] PHENIX collaboration, T. Chujo, *Results on identified hadrons from the PHENIX experiment at RHIC*, *Nucl. Phys. A* **715** (2003) 151 [[nucl-ex/0209027](#)] [[INSPIRE](#)].
- [17] PHENIX collaboration, A. Adare et al., *Energy Loss and Flow of Heavy Quarks in $Au+Au$ Collisions at $\sqrt{s_{NN}} = 200$ GeV*, *Phys. Rev. Lett.* **98** (2007) 172301 [[nucl-ex/0611018](#)] [[INSPIRE](#)].
- [18] STAR collaboration, B.I. Abelev et al., *Erratum: Transverse momentum and centrality dependence of high- p_T non-photon electron suppression in $Au+Au$ collisions at $\sqrt{s_{NN}} = 200$ GeV*, *Phys. Rev. Lett.* **98** (2007) 192301 [*Erratum ibid.* **106** (2011) 159902] [[nucl-ex/0607012](#)] [[INSPIRE](#)].
- [19] ALICE collaboration, *Charged-particle multiplicity density at mid-rapidity in central Pb-Pb collisions at $\sqrt{s_{NN}} = 2.76$ TeV*, *Phys. Rev. Lett.* **105** (2010) 252301 [[arXiv:1011.3916](#)] [[INSPIRE](#)].

- [20] ALICE collaboration, *Elliptic flow of charged particles in Pb-Pb collisions at 2.76 TeV*, *Phys. Rev. Lett.* **105** (2010) 252302 [[arXiv:1011.3914](#)] [[INSPIRE](#)].
- [21] ALICE collaboration, *Suppression of Charged Particle Production at Large Transverse Momentum in Central Pb-Pb Collisions at $\sqrt{s_{NN}} = 2.76$ TeV*, *Phys. Lett. B* **696** (2011) 30 [[arXiv:1012.1004](#)] [[INSPIRE](#)].
- [22] ATLAS collaboration, *Observation of a Centrality-Dependent Dijet Asymmetry in Lead-Lead Collisions at $\sqrt{s_{NN}} = 2.77$ TeV with the ATLAS Detector at the LHC*, *Phys. Rev. Lett.* **105** (2010) 252303 [[arXiv:1011.6182](#)] [[INSPIRE](#)].
- [23] CMS collaboration, *Observation and studies of jet quenching in PbPb collisions at nucleon-nucleon center-of-mass energy = 2.76 TeV*, *Phys. Rev. C* **84** (2011) 024906 [[arXiv:1102.1957](#)] [[INSPIRE](#)].
- [24] D. Forster, *Hydrodynamics Fluctuation, Broken Symmetry and Correlation Function*, Benjamin/Cummings, Menlo Park, CA, U.S.A. (1975).
- [25] H.B. Callen and T.A. Welton, *Irreversibility and generalized noise*, *Phys. Rev.* **83** (1951) 34 [[INSPIRE](#)].
- [26] R. Kubo, *Statistical mechanical theory of irreversible processes. 1. General theory and simple applications in magnetic and conduction problems*, *J. Phys. Soc. Jap.* **12** (1957) 570 [[INSPIRE](#)].
- [27] R.M. Davidson and E. Ruiz Arriola, *Mesonic correlation functions in the NJLS model with vector mesons*, *Phys. Lett. B* **359** (1995) 273 [[INSPIRE](#)].
- [28] A. Andronic, P. Braun-Munzinger, J. Stachel and M. Winn, *Interacting hadron resonance gas meets lattice QCD*, *Phys. Lett. B* **718** (2012) 80 [[arXiv:1201.0693](#)] [[INSPIRE](#)].
- [29] P. Huovinen and P. Petreczky, *QCD Equation of State and Hadron Resonance Gas*, *Nucl. Phys. A* **837** (2010) 26 [[arXiv:0912.2541](#)] [[INSPIRE](#)].
- [30] J.I. Kapusta and C. Gale, *Finite Temperature Field Theory Principle and Applications*, second edition, Cambridge University Press, Cambridge (1996),
- [31] M. LeBellac, *Thermal Field Theory*, Cambridge University Press, Cambridge (1996).
- [32] C. Gale and J.I. Kapusta, *Vector dominance model at finite temperature*, *Nucl. Phys. B* **357** (1991) 65 [[INSPIRE](#)].
- [33] M.G. Mustafa, A. Schafer and M.H. Thoma, *Nonperturbative dilepton production from a quark gluon plasma*, *Phys. Rev. C* **61** (2000) 024902 [[hep-ph/9908461](#)] [[INSPIRE](#)].
- [34] S. Ghosh, S. Sarkar and S. Mallik, *Analytic structure of ρ meson propagator at finite temperature*, *Eur. Phys. J. C* **70** (2010) 251 [[arXiv:0911.3504](#)] [[INSPIRE](#)].
- [35] H.-T. Ding et al., *Thermal dilepton rate and electrical conductivity: An analysis of vector current correlation functions in quenched lattice QCD*, *Phys. Rev. D* **83** (2011) 034504 [[arXiv:1012.4963](#)] [[INSPIRE](#)].
- [36] O. Kaczmarek and A. Francis, *Electrical conductivity and thermal dilepton rate from quenched lattice QCD*, *J. Phys. G* **38** (2011) 124178 [[arXiv:1109.4054](#)] [[INSPIRE](#)].
- [37] A. Francis and O. Kaczmarek, *On the temperature dependence of the electrical conductivity in hot quenched lattice QCD*, *Prog. Part. Nucl. Phys.* **67** (2012) 212 [[arXiv:1112.4802](#)] [[INSPIRE](#)].

- [38] S. Datta, F. Karsch, P. Petreczky and I. Wetzorke, *Behavior of charmonium systems after deconfinement*, *Phys. Rev. D* **69** (2004) 094507 [[hep-lat/0312037](#)] [[INSPIRE](#)].
- [39] G. Aarts, C. Allton, J. Foley, S. Hands and S. Kim, *Spectral functions at small energies and the electrical conductivity in hot, quenched lattice QCD*, *Phys. Rev. Lett.* **99** (2007) 022002 [[hep-lat/0703008](#)] [[INSPIRE](#)].
- [40] G. Aarts and J.M. Martinez Resco, *Transport coefficients, spectral functions and the lattice*, *JHEP* **04** (2002) 053 [[hep-ph/0203177](#)] [[INSPIRE](#)].
- [41] G. Aarts and J.M. Martinez Resco, *Ward identity and electrical conductivity in hot QED*, *JHEP* **11** (2002) 022 [[hep-ph/0209048](#)] [[INSPIRE](#)].
- [42] A. Amato, G. Aarts, C. Allton, P. Giudice, S. Hands and J.I. Skullerud, *Electrical conductivity of the quark-gluon plasma across the deconfinement transition*, *Phys. Rev. Lett.* **111** (2013) 172001 [[arXiv:1307.6763](#)] [[INSPIRE](#)].
- [43] F. Karsch, E. Laermann, P. Petreczky, S. Stickan and I. Wetzorke, *A Lattice calculation of thermal dilepton rates*, *Phys. Lett. B* **530** (2002) 147 [[hep-lat/0110208](#)] [[INSPIRE](#)].
- [44] G. Aarts and J.M. Martinez Resco, *Continuum and lattice meson spectral functions at nonzero momentum and high temperature*, *Nucl. Phys. B* **726** (2005) 93 [[hep-lat/0507004](#)] [[INSPIRE](#)].
- [45] F. Karsch, M.G. Mustafa and M.H. Thoma, *Finite temperature meson correlation functions in HTL approximation*, *Phys. Lett. B* **497** (2001) 249 [[hep-ph/0007093](#)] [[INSPIRE](#)].
- [46] E. Braaten, R.D. Pisarski and T.-C. Yuan, *Production of Soft Dileptons in the quark-gluon Plasma*, *Phys. Rev. Lett.* **64** (1990) 2242 [[INSPIRE](#)].
- [47] C. Greiner, N. Haque, M.G. Mustafa and M.H. Thoma, *Low Mass Dilepton Rate from the Deconfined Phase*, *Phys. Rev. C* **83** (2011) 014908 [[arXiv:1010.2169](#)] [[INSPIRE](#)].
- [48] P. Chakraborty, M.G. Mustafa and M.H. Thoma, *Quark number susceptibility, thermodynamic sum rule and hard thermal loop approximation*, *Phys. Rev. D* **68** (2003) 085012 [[hep-ph/0303009](#)] [[INSPIRE](#)].
- [49] P. Chakraborty, M.G. Mustafa and M.H. Thoma, *Quark number susceptibility in hard thermal loop approximation*, *Eur. Phys. J. C* **23** (2002) 591 [[hep-ph/0111022](#)] [[INSPIRE](#)].
- [50] P. Chakraborty, M.G. Mustafa and M.H. Thoma, *Chiral susceptibility in hard thermal loop approximation*, *Phys. Rev. D* **67** (2003) 114004 [[hep-ph/0210159](#)] [[INSPIRE](#)].
- [51] M. Laine, A. Vuorinen and Y. Zhu, *Next-to-leading order thermal spectral functions in the perturbative domain*, *JHEP* **09** (2011) 084 [[arXiv:1108.1259](#)] [[INSPIRE](#)].
- [52] P. Czerski, *HTL meson correlation functions at finite momentum and chemical potential*, *Nucl. Phys. A* **807** (2008) 11 [[INSPIRE](#)].
- [53] P. Czerski, *Pseudoscalar Meson Temporal Correlation Function in HTL approach*, *Int. J. Mod. Phys. A* **22** (2007) 672 [[hep-ph/0608134](#)] [[INSPIRE](#)].
- [54] W.M. Alberico, A. Beraudo, P. Czerski and A. Molinari, *Finite momentum meson correlation functions in a QCD plasma*, *Nucl. Phys. A* **775** (2006) 188 [[hep-ph/0605060](#)] [[INSPIRE](#)].
- [55] W.M. Alberico, A. Beraudo and A. Molinari, *Meson correlation functions in a QCD plasma*, *Nucl. Phys. A* **750** (2005) 359 [[hep-ph/0411346](#)] [[INSPIRE](#)].
- [56] P.B. Arnold, G.D. Moore and L.G. Yaffe, *Transport coefficients in high temperature gauge theories. 1. Leading log results*, *JHEP* **11** (2000) 001 [[hep-ph/0010177](#)] [[INSPIRE](#)].

- [57] P.B. Arnold, G.D. Moore and L.G. Yaffe, *Transport coefficients in high temperature gauge theories. 2. Beyond leading log*, *JHEP* **05** (2003) 051 [[hep-ph/0302165](#)] [[INSPIRE](#)].
- [58] Y. Burnier and M. Laine, *Massive vector current correlator in thermal QCD*, *JHEP* **11** (2012) 086 [[arXiv:1210.1064](#)] [[INSPIRE](#)].
- [59] M. Laine and M. Vepsäläinen, *Mesonic correlation lengths in high temperature QCD*, *JHEP* **02** (2004) 004 [[hep-ph/0311268](#)] [[INSPIRE](#)].
- [60] T.H. Hansson and I. Zahed, *Hadronic correlators in hot QCD*, *Nucl. Phys. B* **374** (1992) 277 [[INSPIRE](#)].
- [61] N. Haque, J.O. Andersen, M.G. Mustafa, M. Strickland and N. Su, *Three-loop HTLpt Pressure and Susceptibilities at Finite Temperature and Density*, *Phys. Rev. D* **89** (2014) 061701 [[arXiv:1309.3968](#)] [[INSPIRE](#)].
- [62] N. Haque, A. Bandyopadhyay, J.O. Andersen, M.G. Mustafa, M. Strickland and N. Su, *Three-loop HTLpt thermodynamics at finite temperature and chemical potential*, *JHEP* **05** (2014) 027 [[arXiv:1402.6907](#)] [[INSPIRE](#)].
- [63] N. Haque, M.G. Mustafa and M. Strickland, *Quark Number Susceptibilities from Two-Loop Hard Thermal Loop Perturbation Theory*, *JHEP* **07** (2013) 184 [[arXiv:1302.3228](#)] [[INSPIRE](#)].
- [64] N. Haque, M.G. Mustafa and M. Strickland, *Two-loop hard thermal loop pressure at finite temperature and chemical potential*, *Phys. Rev. D* **87** (2013) 105007 [[arXiv:1212.1797](#)] [[INSPIRE](#)].
- [65] B. He, H. Li, C.M. Shakin and Q. Sun, *Comparison of temperature dependent hadronic current correlation functions calculated in lattice simulations of QCD and with a chiral Lagrangian model*, *Phys. Rev. C* **67** (2003) 065203 [[hep-ph/0302105](#)] [[INSPIRE](#)].
- [66] B. He, H. Li, C.M. Shakin and Q. Sun, *Calculation of the pseudoscalar isoscalar hadronic current correlation functions of the quark gluon plasma*, *Phys. Rev. D* **67** (2003) 014022 [[hep-ph/0210387](#)] [[INSPIRE](#)].
- [67] B. He, H. Li, C.M. Shakin and Q. Sun, *Calculation of temperature dependent hadronic correlation functions of pseudoscalar and vector currents*, *Phys. Rev. D* **67** (2003) 114012 [[hep-ph/0212345](#)] [[INSPIRE](#)].
- [68] T. Kunihiro, *Quark number susceptibility and fluctuations in the vector channel at high temperatures*, *Phys. Lett. B* **271** (1991) 395 [[INSPIRE](#)].
- [69] M. Oertel, M. Buballa and J. Wambach, *Meson loop effects in the NJLS model at zero and nonzero temperature*, *Phys. Atom. Nucl.* **64** (2001) 698 [*Yad. Fiz.* **64** (2001) 757] [[hep-ph/0008131](#)] [[INSPIRE](#)].
- [70] K. Fukushima, *Chiral effective model with the Polyakov loop*, *Phys. Lett. B* **591** (2004) 277 [[hep-ph/0310121](#)] [[INSPIRE](#)].
- [71] K. Fukushima, *Relation between the Polyakov loop and the chiral order parameter at strong coupling*, *Phys. Rev. D* **68** (2003) 045004 [[hep-ph/0303225](#)] [[INSPIRE](#)].
- [72] R.D. Pisarski, *Quark gluon plasma as a condensate of SU(3) Wilson lines*, *Phys. Rev. D* **62** (2000) 111501 [[hep-ph/0006205](#)] [[INSPIRE](#)].
- [73] A. Dumitru and R.D. Pisarski, *Degrees of freedom and the deconfining phase transition*, *Phys. Lett. B* **525** (2002) 95 [[hep-ph/0106176](#)] [[INSPIRE](#)].

- [74] A. Dumitru and R.D. Pisarski, *Two point functions for SU(3) Polyakov loops near T_c* , *Phys. Rev. D* **66** (2002) 096003 [[hep-ph/0204223](#)] [[INSPIRE](#)].
- [75] A. Dumitru, Y. Hatta, J. Lenaghan, K. Orginos and R.D. Pisarski, *Deconfining phase transition as a matrix model of renormalized Polyakov loops*, *Phys. Rev. D* **70** (2004) 034511 [[hep-th/0311223](#)] [[INSPIRE](#)].
- [76] D.J. Gross, R.D. Pisarski and L.G. Yaffe, *QCD and Instantons at Finite Temperature*, *Rev. Mod. Phys.* **53** (1981) 43 [[INSPIRE](#)].
- [77] A. Gocksch and R.D. Pisarski, *Partition function for the eigenvalues of the Wilson line*, *Nucl. Phys. B* **402** (1993) 657 [[hep-ph/9302233](#)] [[INSPIRE](#)].
- [78] N. Weiss, *The Effective Potential for the Order Parameter of Gauge Theories at Finite Temperature*, *Phys. Rev. D* **24** (1981) 475 [[INSPIRE](#)].
- [79] N. Weiss, *The Wilson Line in Finite Temperature Gauge Theories*, *Phys. Rev. D* **25** (1982) 2667 [[INSPIRE](#)].
- [80] S.K. Ghosh, T.K. Mukherjee, M.G. Mustafa and R. Ray, *Susceptibilities and speed of sound from PNJL model*, *Phys. Rev. D* **73** (2006) 114007 [[hep-ph/0603050](#)] [[INSPIRE](#)].
- [81] S. Mukherjee, M.G. Mustafa and R. Ray, *Thermodynamics of the PNJL model with nonzero baryon and isospin chemical potentials*, *Phys. Rev. D* **75** (2007) 094015 [[hep-ph/0609249](#)] [[INSPIRE](#)].
- [82] S.K. Ghosh, T.K. Mukherjee, M.G. Mustafa and R. Ray, *PNJL model with a Van der Monde term*, *Phys. Rev. D* **77** (2008) 094024 [[arXiv:0710.2790](#)] [[INSPIRE](#)].
- [83] C. Ratti, M.A. Thaler and W. Weise, *Phases of QCD: Lattice thermodynamics and a field theoretical model*, *Phys. Rev. D* **73** (2006) 014019 [[hep-ph/0506234](#)] [[INSPIRE](#)].
- [84] S.K. Ghosh, A. Lahiri, S. Majumder, M.G. Mustafa, S. Raha and R. Ray, *Quark Number Susceptibility: Revisited with Fluctuation-Dissipation Theorem in mean field theories*, *Phys. Rev. D* **90** (2014) 054030 [[arXiv:1407.7203](#)] [[INSPIRE](#)].
- [85] H. Hansen, W.M. Alberico, A. Beraudo, A. Molinari, M. Nardi and C. Ratti, *Mesonic correlation functions at finite temperature and density in the Nambu-Jona-Lasinio model with a Polyakov loop*, *Phys. Rev. D* **75** (2007) 065004 [[hep-ph/0609116](#)] [[INSPIRE](#)].
- [86] P. Deb, A. Bhattacharyya, S. Datta and S.K. Ghosh, *Mesonic Excitations of QGP: Study with an Effective Model*, *Phys. Rev. C* **79** (2009) 055208 [[arXiv:0901.1992](#)] [[INSPIRE](#)].
- [87] S. Carignano, D. Nickel and M. Buballa, *Influence of vector interaction and Polyakov loop dynamics on inhomogeneous chiral symmetry breaking phases*, *Phys. Rev. D* **82** (2010) 054009 [[arXiv:1007.1397](#)] [[INSPIRE](#)].
- [88] K. Kashiwa, H. Kouno, T. Sakaguchi, M. Matsuzaki and M. Yahiro, *Chiral phase transition in an extended NJLS model with higher-order multi-quark interactions*, *Phys. Lett. B* **647** (2007) 446 [[nucl-th/0608078](#)] [[INSPIRE](#)].
- [89] Y. Sakai, K. Kashiwa, H. Kouno, M. Matsuzaki and M. Yahiro, *Vector-type four-quark interaction and its impact on QCD phase structure*, *Phys. Rev. D* **78** (2008) 076007 [[arXiv:0806.4799](#)] [[INSPIRE](#)].
- [90] K. Fukushima, *Phase diagrams in the three-flavor Nambu-Jona-Lasinio model with the Polyakov loop*, *Phys. Rev. D* **77** (2008) 114028 [*Erratum ibid.* **D 78** (2008) 039902] [[arXiv:0803.3318](#)] [[INSPIRE](#)].

- [91] K. Fukushima, *Critical surface in hot and dense QCD with the vector interaction*, *Phys. Rev. D* **78** (2008) 114019 [[arXiv:0809.3080](#)] [[INSPIRE](#)].
- [92] R.Z. Denke, J.C. Macias and M.B. Pinto, *Critical Line Back-Bending Induced either by Finite N_c Corrections or by a Repulsive Vector Channel*, *J. Mod. Phys.* **4** (2013) 1583.
- [93] P. Jaikumar, R. Rapp and I. Zahed, *Photon and dilepton emission rates from high density quark matter*, *Phys. Rev. C* **65** (2002) 055205 [[hep-ph/0112308](#)] [[INSPIRE](#)].
- [94] N. Haque, M.G. Mustafa and M.H. Thoma, *Conserved Density Fluctuation and Temporal Correlation Function in HTL Perturbation Theory*, *Phys. Rev. D* **84** (2011) 054009 [[arXiv:1103.3394](#)] [[INSPIRE](#)].
- [95] Y. Nakahara, M. Asakawa and T. Hatsuda, *Hadronic spectral functions in lattice QCD*, *Phys. Rev. D* **60** (1999) 091503 [[hep-lat/9905034](#)] [[INSPIRE](#)].
- [96] M. Asakawa, T. Hatsuda and Y. Nakahara, *Maximum entropy analysis of the spectral functions in lattice QCD*, *Prog. Part. Nucl. Phys.* **46** (2001) 459 [[hep-lat/0011040](#)] [[INSPIRE](#)].
- [97] I. Wetzorke and F. Karsch, *Testing MEM with diquark and thermal meson correlation functions*, [hep-lat/0008008](#) [[INSPIRE](#)].
- [98] S.P. Klevansky, *The Nambu-Jona-Lasinio model of quantum chromodynamics*, *Rev. Mod. Phys.* **64** (1992) 649 [[INSPIRE](#)].
- [99] T. Hatsuda and T. Kunihiro, *QCD phenomenology based on a chiral effective Lagrangian*, *Phys. Rept.* **247** (1994) 221 [[hep-ph/9401310](#)] [[INSPIRE](#)].
- [100] M. Buballa, *NJLS model analysis of quark matter at large density*, *Phys. Rept.* **407** (2005) 205 [[hep-ph/0402234](#)] [[INSPIRE](#)].
- [101] C.A. Islam, R. Abir, M.G. Mustafa, S.K. Ghosh and R. Ray, *The consequences of SU(3) color singletness, Polyakov Loop and Z(3) symmetry on a quark-gluon gas*, *J. Phys. G* **41** (2014) 025001 [[arXiv:1208.3146](#)] [[INSPIRE](#)].
- [102] A. Das, *Finite Temperature Field Theory*, World scientific (1997).
- [103] C. Gale et al., *Production and Elliptic Flow of Dileptons and Photons in the semi-Quark Gluon Plasma*, [arXiv:1409.4778](#) [[INSPIRE](#)].
- [104] A. Bazavov et al., *The chiral and deconfinement aspects of the QCD transition*, *Phys. Rev. D* **85** (2012) 054503 [[arXiv:1111.1710](#)] [[INSPIRE](#)].
- [105] P. Petreczky, *Numerical study of hot strongly interacting matter*, *J. Phys. Conf. Ser.* **402** (2012) 012036 [[arXiv:1204.4414](#)] [[INSPIRE](#)].
- [106] WUPPERTAL-BUDAPEST collaboration, S. Borsányi et al., *Is there still any T_c mystery in lattice QCD? Results with physical masses in the continuum limit III*, *JHEP* **09** (2010) 073 [[arXiv:1005.3508](#)] [[INSPIRE](#)].